James Webb Space Telescope Project

Integrated Science Instrument Module

NIRCam0077 – Redacted
Radiation Testing of a NIRCam 5-micron Cutoff Sensor Chip Assembly

Lisa May Walker*, Christina Williams, and Marcia Rieke
University of Arizona,
Jean-Marie Lauenstein
Flight Data Systems and Radiation Effects Branch
Bernard J. Rauchser
JWST Science Office
NASA/GSFC
Robert McMurray
Ames Research Center
*Walker now works for GEOST, Inc.

April 10, 2018

Table of Contents

List of Figures

List of Tables

SUMMARY

A JWST flight-build 5-micron cut-off sensor chip assembly (SCA, also referred to as an "array" or "detector") was exposed to 8.25 and 63MeV protons at the University of California Davis cyclotron. A suite of detector performance properties were measured before and after irradiation with the array kept at 37K for a month after the last proton exposure. Dark current returned to close to the pre-exposure levels in less than 24-hours. A small number of pixels (0.7%) were permanently damaged sowing elevated dark current as a result of the radiation exposure. Response to the 0.95 micron LED mounted inside the Ames test dewar did not change after exposure to 8.25 MeV radiation, but nominally showed a drop of ~10% after exposure to 63 MeV radiation with the average response level still increasing a month after the exposure. No obvious clocking failures were seen so there were no single event upsets in the detector readout circuitry.

1 INTRODUCTION

A five-micron cut-off array that was fabricated as part of the NIRCam flight build after the barrier-layer improvement was selected for use in radiation testing at the University of California Davis Cyclotron. Table 1 gives the basic properties for SCA 17159 based on Arizona test data except for the quantum efficiency and transimpedance gain which were measured at Teledyne. Figure 1 shows both dark and illuminated images with the large dark region in the dark image being an "epoxy void". Epoxy voids are common in the JWST flight build parts. Also apparent in Figure 1 are the cosmetic flaws which caused this part to be categorized as non-flight. Appendix B describes the procedures followed in measuring these values.

For these tests, the SCA was mounted in a dewar provided by Dr. Robert McMurray of NASA Ames Research Center. Dr. McMurray mounted the detector in the dewar, and he also provided the readout electronics and data acquisition scripts.

The H2RG detectors used on JWST instruments are read out non-destructively with the readout pattern consisting of a pixel-by-pixel reset followed by reading the output voltage level of each pixel every 10.7 seconds. For this test discussion among participants and GSFC led to reading out only one quarter of an array which gave a shorter sampling period of ~5.2 seconds. The region that was readout consisted of half of each of two of the four "stripes" in an H2RG so two separate H2RG output amplifiers were included in the signal chain as well as reference pixels and all of the required clocking registers. Figure 2 delineates the region read out. The testing used ramps with either eight or sixteen

Table 1: Properties of the Test SCA (17159)

SCA	Full Well e-	QE(3.5 µm)	CDS e-	Idk (36.5K) e-/sec	Total Noise (1000s) e-	Transimpedance gain µV/e-
17159	90000	0.84	14.9	0.029	8.4	4.46

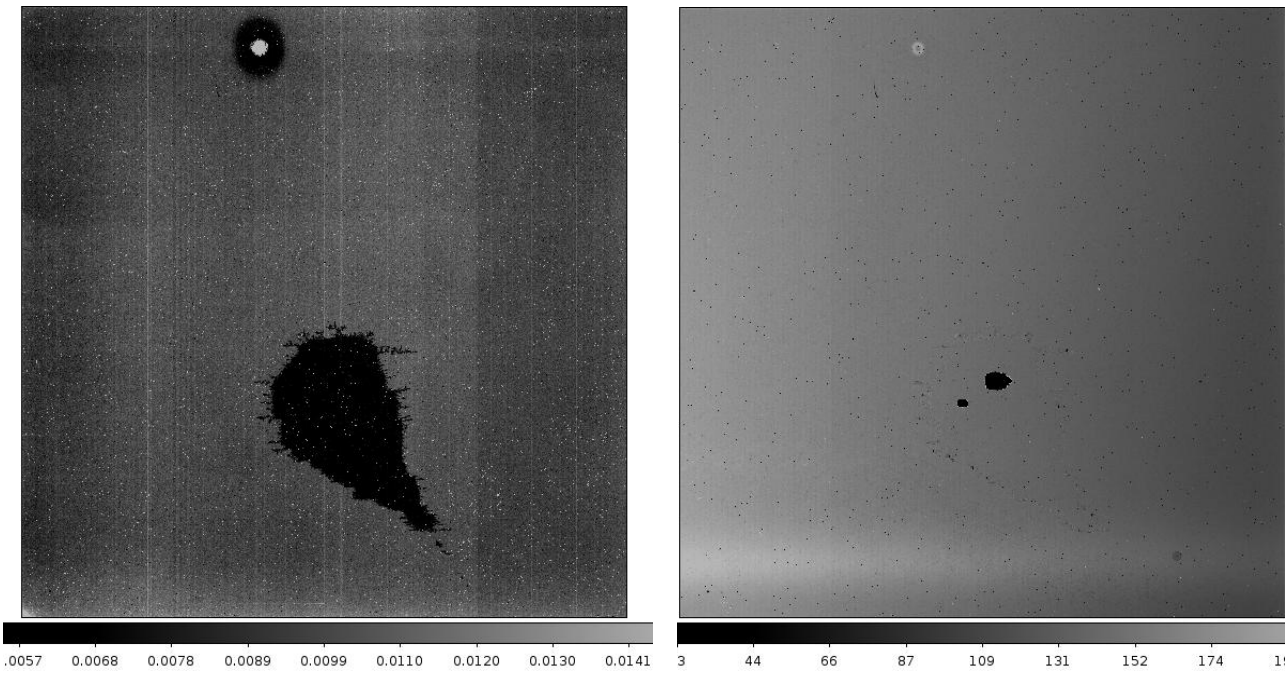

Figure 1: A dark image (left) and an illuminated image (right) of SCA 17159. The gray scale units are DN/sec for the Arizona test set-up and should be multiplied by 2.7 to convert to e-/sec.

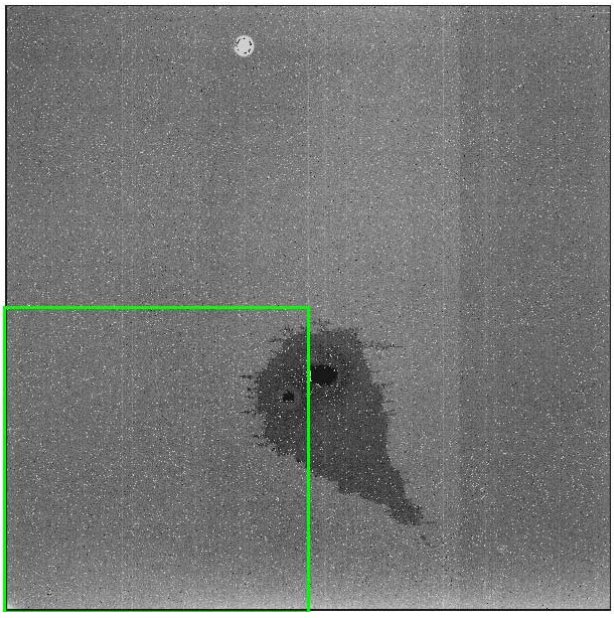

Figure 2: The green box outlines the region read out during the radiation tests.

reads (referred to as frames in JWST nomenclature but not to be confused the Ames usage of "frame" designating an entire ramp) between resets. Figure 3 presents ramps with illumination from the dewar's internal LED showing how charge accumulates during an exposure. Also shown is a linear fit to one of the ramps. This type of fit is one of the standard signal extraction methods used in this report, and forms the backbone of the JWST data pipelines. The slope of the fit is the desired signal, and is expressed in electrons/second.

Figure 4 shows an average ramp for a typical pixel in the dark before irradiation, and the first read after reset has an average value higher than the rest of the ramp. The second read is also somewhat higher. The first read in a ramp was not used in any of the analyses here, and subtle differences in the readout timing (eg., readout electronics at slightly different temperatures) can cause the magnitude of the first read effect to vary, and contributes to the negative slopes observed during these tests.

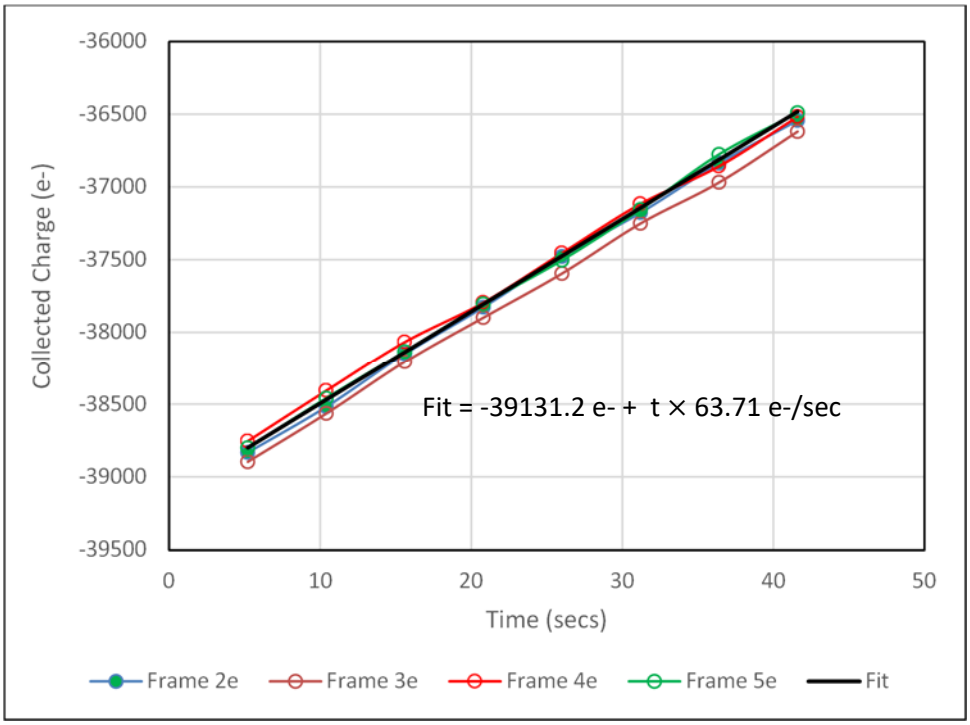

Figure 3: Sample ramps from LED-illuminated data.

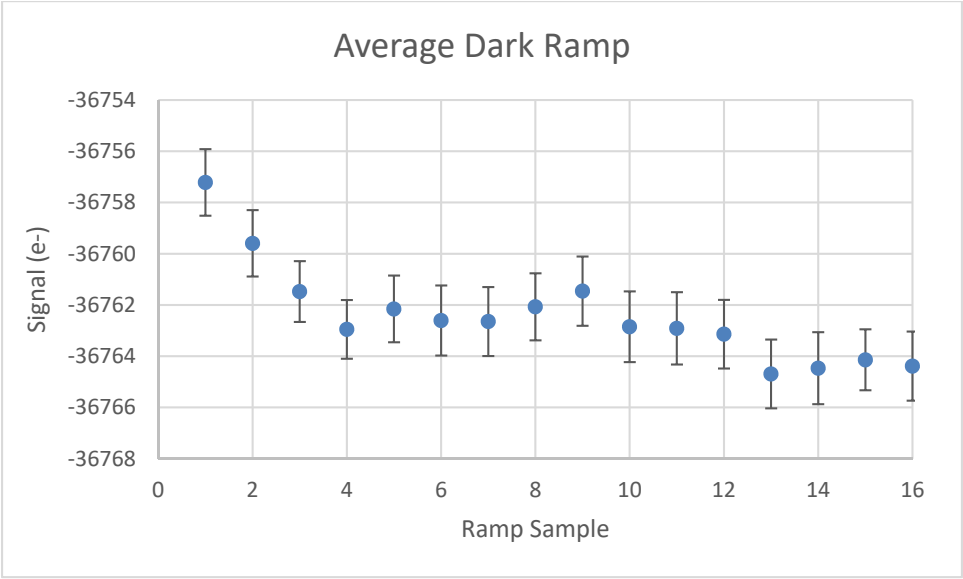

Figure 4: Average ramp for pixel 500,500 before irradiation. The error bars indicate the spread in values after removing the kTC reset variations.

Another contributor to the production of negative slopes is the read noise of the Ames electronics as compared to the intrinsic dark current of the detector. The dark current for this array as reported in Table 1 from testing in at Arizona using 1696-second ramps is 0.029 e-/sec. The longest ramps used for data taken with the Ames system are 16 reads x 5.2 secs/read = 83.2 seconds. In a ramp of this length only 0.029 e-/sec x 83.2 = 2.4 e- will be collected on average from the dark current. Table 2 presents the read noise for the Ames system measured from dark data and from data with no bias across the detector. Because only modest numbers of ramps were available for read noise estimation, there is a

spread in values. We adopt 14e- as the read noise floor. A noise of 14 electrons in 83.2 seconds is equivalent to a slope uncertainty of 14 e- / 83.2 seconds = 0.17 e-/sec, much larger than the intrinsic read noise which in turn leads to some pixels have apparently negative slopes in dark data. Read noise post-irradiation appears better because of better statistics but is certainly no worse than before irradiation.

Table 2: Read Noise

Type of data	Read noise (e-)	Slope Uncertainty (e-/sec)	No. of Samples	Location
8-frame ramps	13.7	0.33	45	Ames
16-frame ramps	15.8	0.19	12	UC Davis
Double-correlated sampling	12.0	N/A	30	Ames
Zero bias, 8-frame (DSUB=VRESET=0.25)	16.6	0.40	5	Ames
Zero bias, 8-frame (DSUB=VRESET=0.30)	22.5	0.54	30	4 at Davis, 26 at Ames
Feb 19 post-irradiation	10.9	.131	53	At Ames

Table 3: Detector Biases

Bias	Volts
Vdd	3.30
Dsub	0.50
Vreset	0.25
Vbiasgate	2.26
Drain	0.01
Celldrain	0.01
Vbiaspower	3.20
Vdda	3.30

2 PROCEDURE

The array was clocked using the same pixel clock (10 μsec per pixel) and waveforms as would be used in a JWST data collection system. The array was used in buffered, high-power mode which was a necessity due to the lack of a SIDECAR ASIC and the relatively long cabling to the readout electronics. The detector was biased using the same set of biases as used for testing at Arizona, and which will be used on orbit. The biases are listed in Table 3. The use of only 8 or 16-sample ramps limited the ultimate read noise achieveable as described above. The read noise of 8.4 e- measured at Arizona was derived in 1000-seconds which has a disadvantage when any cause such as charge particles is depositing charge in a pixels as saturation is more likely.

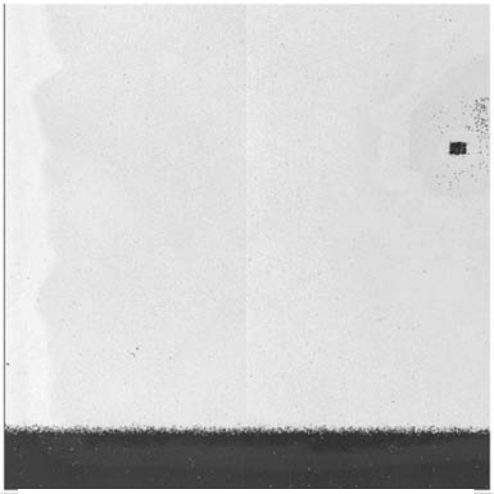

Figure 5: An image taken when the beam was turned on during the read.

The test dewar did not include a system for recording the detector temperature. The temperature was controlled using a Lakeshore Controller which stabilized the cold stage temperature including the array at 37 K and maintained this temperature throughout test period. The Lakeshore and cold stage heater were run on a UPS during transport to and from the Davis accelerator. The array was cooled down to 37 K on February 4, 2015, and pre-irradiation data were acquired on four days including after transport to the Davis Cyclotron but before subjecting the detector to radiation on February 9, 2015. The detector was kept at 37 K until March 20, 2015, 30 days after the last irradiation to enable distinguishing recovery from irradiation due to time from recovery due to temperature annealing.

The H2RG detector was irradiated with a beam of protons on two

separate days (Feb 9 and 18, 2015). On Feb 9, the beam energy when arriving at the detector was 8.25 MeV. On Feb 18, the beam energy was increased to 63 MeV when arriving at the detector. This range of energies gives an indication of the range of effects that radiation at L2 might induce in JWST detectors. The test parameters are including the Total Ionizing Doses of 5.21 krad (Si) at 8.25 MeV and 6.93 krad (Si) at 63 MeV. Some runs were taken at low rates to be used in pipeline testing. On both days, the dewar was exposed to the beam 3 times. The first time, "sprinkles", the flux was very low; this was to allow for detection of individual hits. The second and third times the flux was increased to investigate possible damage to detector from the radiation. Figure 5 show an image when the full beam level came on during the read. Once the cyclotron was delivering the full power used in these tests, the pixels were fully saturated by the charge deposited by the protons nearly instantaneously. By agreement before the testing, only 25% of the detector was read during and after the exposure to the beam consisting of the bottom half of the detector and the sections read by amplifier 1 and amplifier 2 as shown in Figure 2. This yielded frames of 1024x1024 pixels

2.1 ANALYSIS

2.1.1 Data Reduction

The Ames readout electronics record the data in volts. To convert to electrons, each raw ramp was multiplied by a factor of 25500 e- /volt. This factor is based on the gain of 8.8 for Ames video amplifier and analogue-to-digital converter and the transimpedance gain for this array of 4.46 μV/e- provided by Teledyne. This agrees well with the nominal gain of 23000 e-/V for an H2RG used by Dr. McMurray for a nominal transimpedance gain of ~4.9 μV/e-.

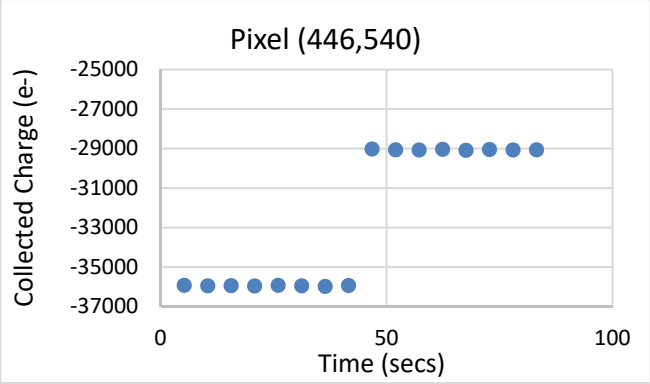

Figure 6: A sample hit from one of the 8.25 MeV "sprinkle" runs.

Two types of analysis were performed. One used in looking at changes in response to light from the LED and in looking at changes in the dark current was the linear fit as described in the introduction. Linear fits were performed both with and without reference pixel corrections. The corner readout configuration used for these tests has fewer reference pixels relative to the number of light sensitive pixels than when full frame reads are used, and the read noise was higher using a reference pixel correction so such corrections were not used.

The other type of analysis used was one for detecting radiation hits. Figure 6 shows how a hit produces a jump in the level with the size of the jump being equal to the amount of charge deposited by the hit. As described below, hit searches rely on looking at differences computed between successive reads. Any jumps in the DC level of pixels (eg. from noise on bias lines) will look like radiation hits so reference pixel corrections were performed for this analysis. Reference pixels are affected by bias changes just as light-sensitive pixels are so bias jumps are effectively removed by using the reference pixels. For each amplifier, a resistant mean (computed after removing pixels more than 5-sigma from the initial mean) was calculated for the bottom four rows of pixels across all frames and was then subtracted from all pixels read out by that amplifier. For the side pixels, a row-by-row mean was calculated for the first four rows of pixels across all reads and then subtracted from all pixels in that row. Once the reference pixel correction was performed, a two-point-difference ramp was then calculated by subtracting each read from the read after it. The output ramp used to identify hits was

1020x1020 detector pixels xN_{reads}-1. The 50 edge pixels were ignored in hit detection to mitigate potential edge effects (incomplete beam coverage, reset issues, etc).

To search for hits, the mean and standard deviation of the entire set of two-point-differences from a ramp were calculated with the largest difference removed for each pixel removed from the calculation. A potential hit was identified if that largest difference was greater than the mean by at least 5x the standard deviation for the entire ramp. A hit map was generated for each ramp to identify the hit pixels for subsequent analysis.

Before a potential hit was determined to be an actual hit, checks were performed to ensure that it wasn't a hot pixel or random telegraph noise (RTN). The hot pixel check was performed against a list of hot pixels generated from data taken before any irradiation of the array. Jumps due to random telegraph noise were eliminated if the pixel jumped in the negative direction in the same ramp. A small percentage hits due to RTN jumps will be misidentified as charge particle hits because there is no way to screen for them if there is not a corresponding negative jump. Prior testing of NIRCam parts indicates that in long ramps ~0.02% of the pixels in a full frame will be affected by RTN so this presents an upper limit to the number of such mid-identified hits at ~50 hits per 1020x1020 area. A better limit comes from the hit rates at measured at Ames where the most accurate rate come s from the data taken at the very end of the test when radiation effects had largely decayed away. This rate determined from 91 dark ramps taken on March 20, 2015, is 31.1 hits per 1020x1020 pixel region per read up the ramp, equivalent to 0.003% of the hits.

2.2 POST-CYCLOTRON HIT RATES

Because materials in the test dewar and array mounting can be activated by proton exposure, the hit maps described earlier were used to measure the hit rate as a function of time. To determine the hit rate, pixels identified as hits in the hit map were used. Pixels which were < 1.5% of the signal of a neighboring pixel, a possible indication of inter-pixel capacitance, were excluded. For each ramp, the number of hit pixels was counted to determine how long after the radiation exposure hits were detected. As shown Figure 7, the number of hit pixels tapers off with time, such that by the end of the testing period the rate of hits is similar to the pre-radiation data. Note that the units here are number of hits per read, not pre ramp. The activation from the 8.25 MeV exposure decayed more quickly than from the 63 MeV exposure. Figure 8 and Figure 9 show the hit rates close in time to the two proton exposures.

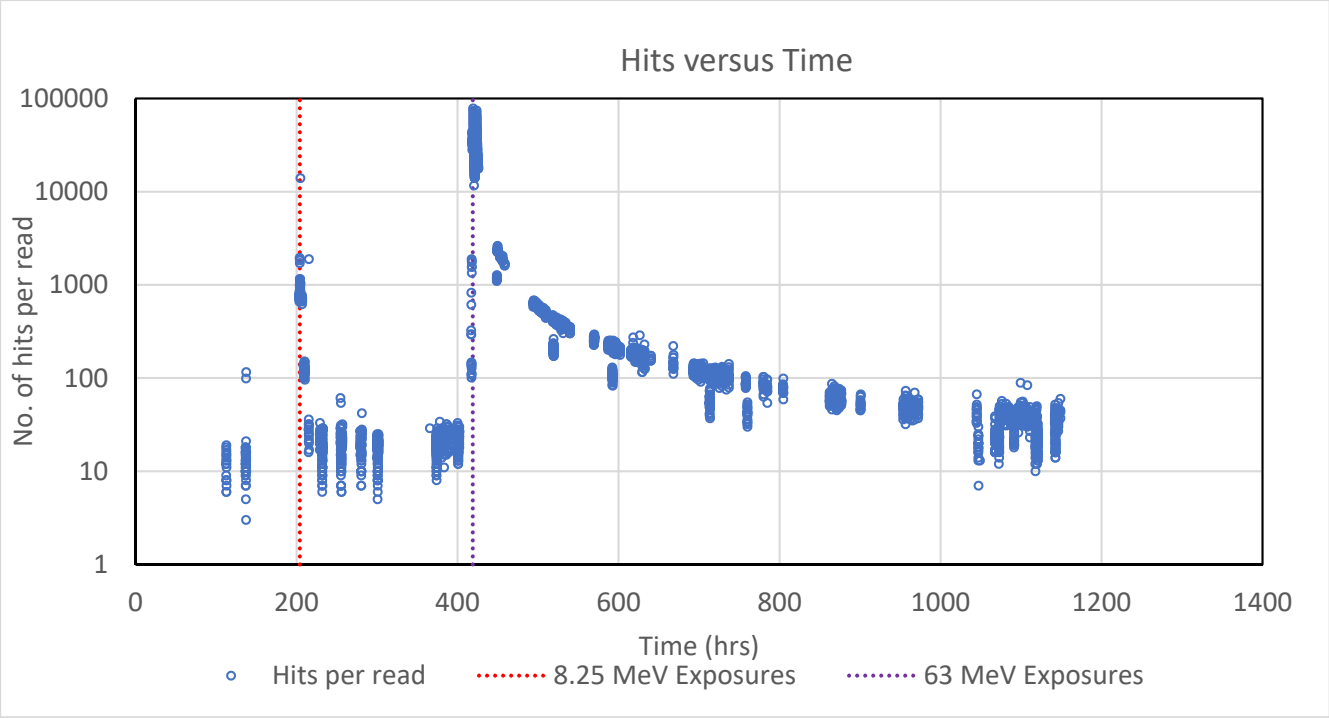

Figure 7: The number of hit pixels in a ramp as a function of date.

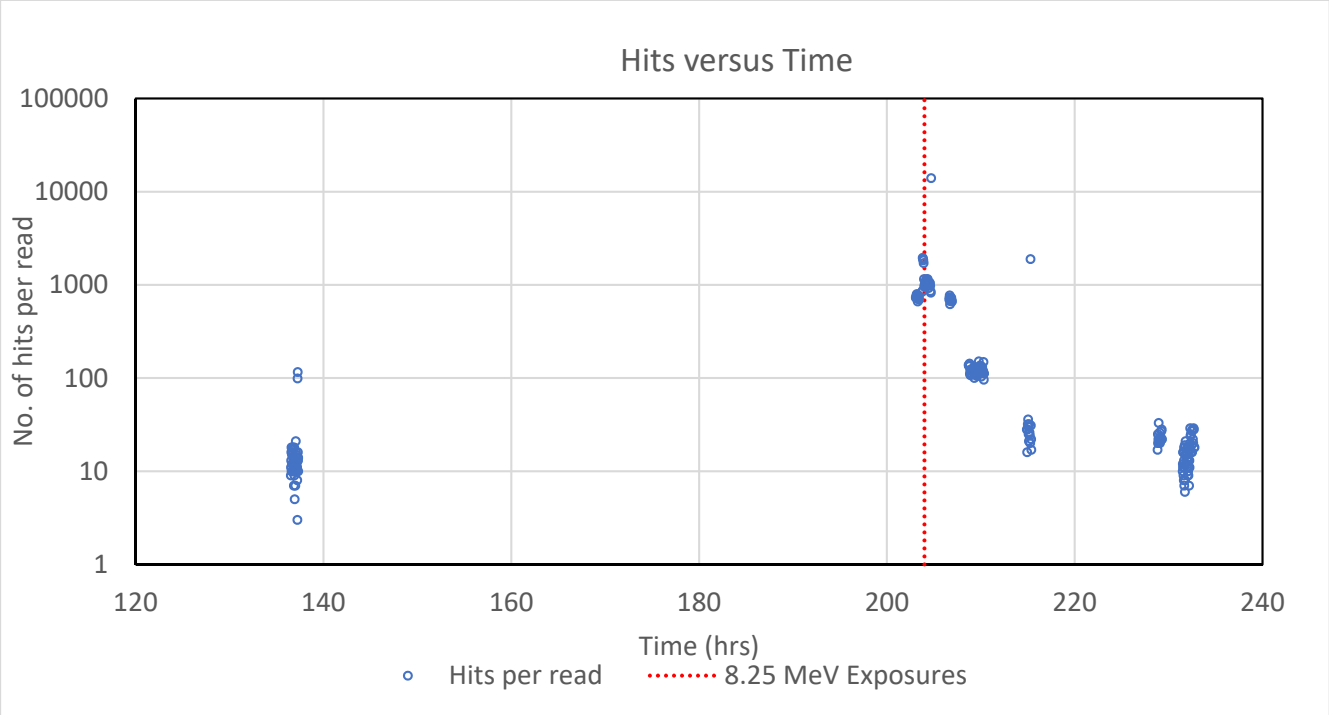

Figure 8: Portion of Figure **7** near the time of 8.25 MeV irradation.

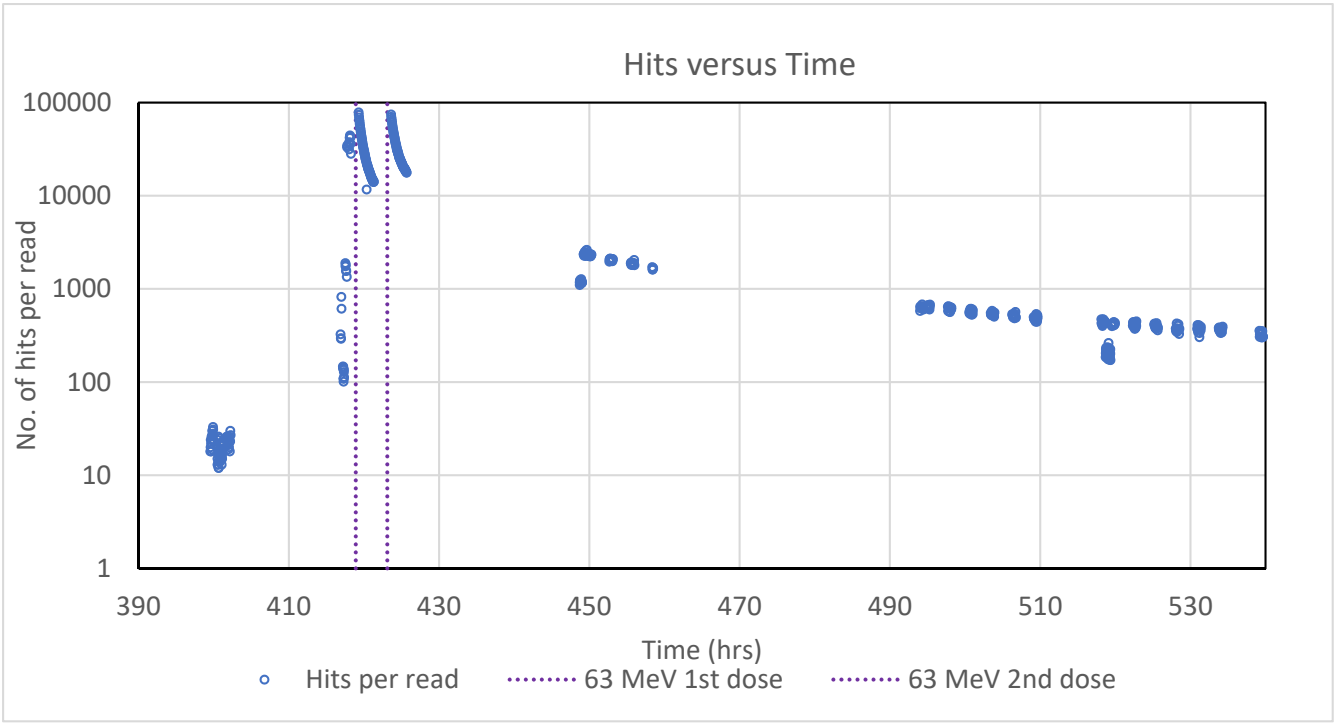

Figure 9: Portion of Figure **7** near the time of 63 MeV irradiation.

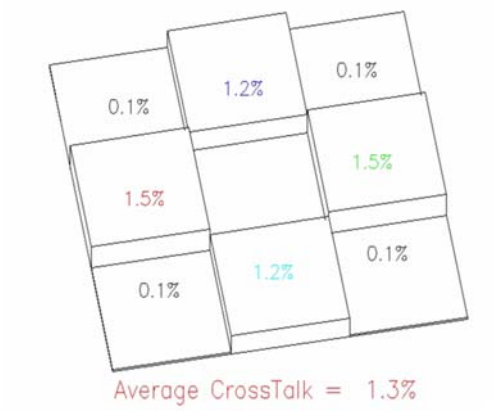

Figure 10: Crosstalk as measured by Teledyne due to inter-pixel capacitance for 17159.

3 RESULTS

3.1 INDUCED CHARGES OR CHARGE SPREADING

Figure 10 shows the crosstalk between a central pixel and surrounding pixels due to interpixel capacitance (eg. Donlon et al., Proceedings of the SPIE, Volume 9915, id. 99152I 8 pp. 2016 and references therein). The low hit rate images were examined to see whether the proton hits induced similar scale charges in the pixels surrounding a hit. A sample of single hit pixels were chosen by eye from the low hit rate data sets at both 8 MeV and 63 MeV to examine in detail possible charge spreading and recovery of slopes before and after a hit. Pixels hit between reads 8 and 9 were chosen for examination as this choice left enough pixels before and after the hit to compute a slope. The 8 MeV sample was chosen from the Feb 09, 2015, 37K_4, Picture 4, Frame 1 image ramp. The 63 MeV sample was chosen from the Feb 18, 2015, 37K_4, Picture 2, and a second set from Picture 3. The "sprinkle" rate at 63 MeV was more than 10x the "sprinkle" rate at 8.25 MeV so care was needed to guard against picking pixels with two hits per ramp.

3.1.1 Induced Charge Behavior from 8 MeV Data

A sample of pixels with isolated hits (meaning with no hits within a radius of ~10 pixels) and which appear symmetric by eye when examined using ds9 was selected. Table 4 lists the selected pixels including the size of the hit**.** Figure 11 presents gray scale images of the hits. The table also lists the

difference between the last pre-hit read and the last read in the ramp. There is a slight tendency for the final read to show a slightly smaller hit size, but the difference is of low statistical significance. Slopes before and after the hit were computed and tabulated as were slopes for the same ranges of reads in a pre-irradiation ramp. These data are inconclusive as to whether pre- and post-hit data in a ramp can be combined. For comparison, slopes were also computed from pre-irradiation ramps using samples 2 through 7 for the "before" slope, and 10 to 16 for the "after" slope. The uncertainties tabulated are the slope uncertainties using a set of 12 ramps before irradiation.

Table 4: Sample Pixel Hits, 8 MeV

Number	Pixel	read 9 – read 8 (e-)	read 16 – read 8 (e-)	Slope Before (e-/sec)	Slope after (e-/sec)	No hit slope before	No hit slope after
1	(446, 540)	6910	6864	-1.45	-0.18	-0.62±0.74	0.39±0.67
2	(471, 857)	6490	6479	-1.58	1.00	0.34±0.97	0.11±0.81
3	(751, 561)	2766	2729	-0.61	-0.54	0.48±0.86	-0.19±1.03
4	(811, 216)	5523	5523	-1.16	0.72	-0.72±0.91	0.22±0.64
5	(939, 289)	4052	4005	0.17	-0.87	-0.12±0.63	-0.61±0.75
6	(296, 293)	15425	15425	-0.80	0.19	-0.34±0.61	0.12±0.90
7	(761, 296)	3718	3737	-0.44	-1.16	-0.08±1.48	0.23±1.07
8	(635, 97)	7714	7702	1.33	-1.59	0.11±0.86	0.27±0.85

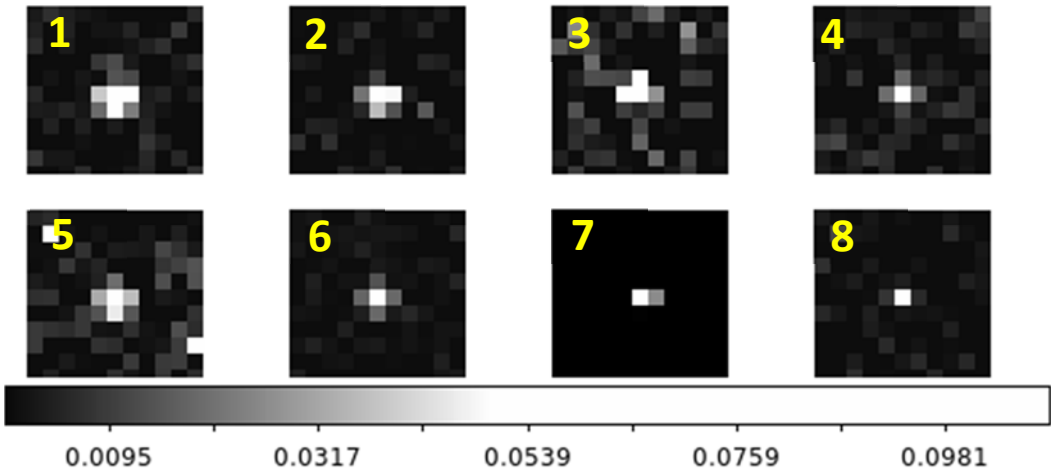

Figure 11: Grayscale images of the 8 hits in the 8 MeV sample.

All eight hits were averaged and a single image was produced to look for charge induced in surrounding pixels. Figure 12 shows the average image from the differences between read 9 and read 8 with the hit occurring sometime during the 5.2-second interval between read 8 and read 9. The figure also shows the average image from combining the differences between read 8 and read 16. By eye the images appear very similar, and Table 5 and Table 6 present the values normalized to unity on the hit itself. Only the values in yellow are statistically significant from 0, and they agree well with the values in Figure 10. For these data, there is no evidence of any induced charge effects beyond that expected from the deposition of charge in a pixel and interpixel capacitance.

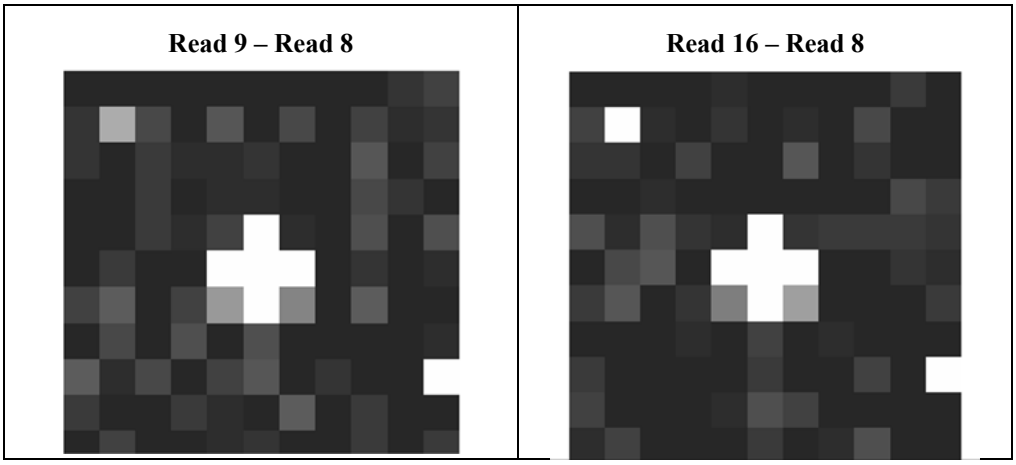

Figure 12: Combined averages of the 8 MeV sample hits.

Table 5: Pixel Values Surrounding the hit pixel from the read immediately after the hit at 8 MeV. σ = +/-0.0051					
	1	2	3	4	5
1	-0.005	-0.00005	-0.0001	-0.003	-0.004
2	-0.0003	0.001	0.019	-0.0002	-0.002
3	-0.004	0.024	1	0.032	-0.003
4	0.001	0.008	0.034	0.007	-0.001
5	0.003	-0.004	0.002	-0.002	-0.002

Table 6: Pixel Values Surrounding the hit pixel from the read 42 seconds after the hit. σ = +/-0.0053					
	1	2	3	4	5
1	-0.001	-0.002	-0.001	-0.003	-0.004
2	0.00007	-0.0004	0.015	0.0005	0.0007
3	-0.007	0.021	1	0.032	-0.003
4	0.00003	0.006	0.035	0.008	-0.003
5	-0.0005	-0.002	0.001	-0.004	-0.0001

3.1.2 Induced Charge Behavior from 63 MeV Data

The 63 MeV samples were chosen from the Feb 18, 2015, 37K_4, Picture 2 image ramp and from Picture 3. The selection and analyses were identical to those used or the 8.25 MeV data. Table 11 and Table 12 present limited evidence for some induced charge larger than just the levels expected from interpixel capacitance, but even in this case, the only induced charge is in the immediately adjacent pixels which are the ones affected by interpixel capacitance.

Table 7: Sample Pixel Hits from Picture 2, 63 MeV							
Number	Pixel	read 9 – read 8 (e-)	read 16 – read 8 (e-)	Slope Before (e-/sec)	Slope After (e-/sec)	No hit Before	No hit After
1	(99,972)	8237	7831	1.28	-7.54	-0.04±0.88	0.38±0.85
2	(206,924)	11298	11187	14.59	0.04	0.29±1.25	-0.04±0.64
3	(429,896)	17266	17095	-0.48	-4.83	-0.08±0.95	-0.08±0.76
4	(507,876)	25834	25928	-4.17	0.75	-0.16±1.00	0.24±0.74
5	(701,778)	16889	17325	-6.69	-37.26	-0.08±0.82	0.07±0.72
6	(629,628)	22745	22865	-6.89	-6.86	0.91±0.86	-0.36±0.33
7	(419,549)	22331	22665	-16.69	3.60	0.55±1.12	-0.17±0.71
8	(328,417)	13938	13803	-5.87	-9.70	-0.92±1.25	0.28±0.79
9	(407,341)	12708	13146	45.41	8.90	-0.58±1.30	-0.42±0.84
10	(295,279)	9529	9352	16.31	-6.44	-0.86±0.83	-0.31±0.46
11	(155,266)	14908	14809	-7.52	-0.46	0.20±1.25	0.19±0.46
12	(389,168)	21167	21958	12.34	10.42	-0.45±1.14	0.21±0.62
13	(716,204)	14465	14101	-4.46	-3.18	0.31±0.49	1.12±0.96
14*	(763,134)	3803	3574	-3.41	4.10	-0.17±0.96	0.91±1.26
15	(907,398)	32177	32122	-6.97	4.24	-0.02±0.72	-0.31±0.59
16	(765,416)	13149	12550	-13.16	6.47	-0.04±0.98	0.29±0.75

*Not used in the analysis as four pixels were hit with nearly equal charge deposition. Largest charge is reported here.

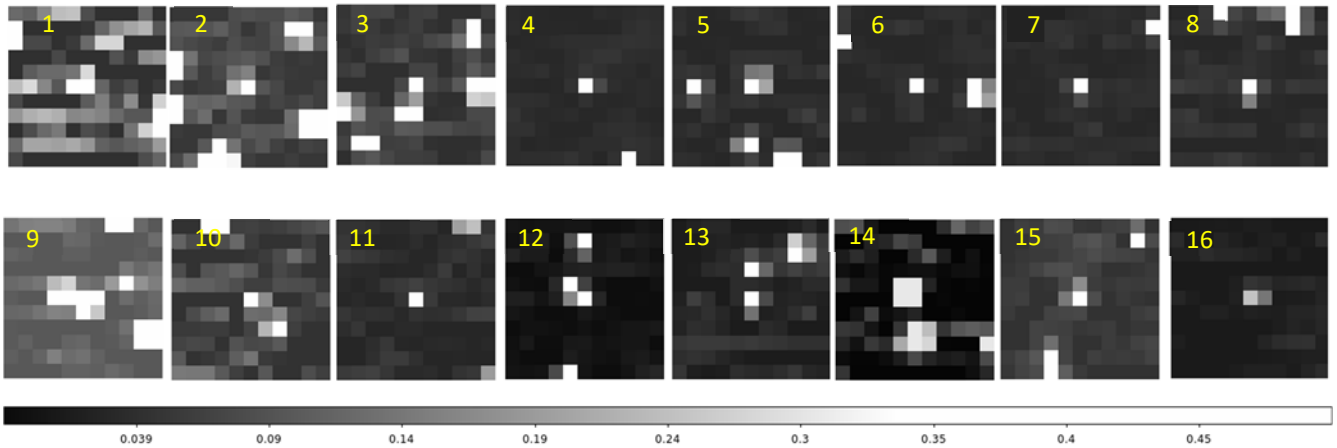

Figure 13: Grayscale images of the 16 hits in the 63 MeV sample from Picture 2.

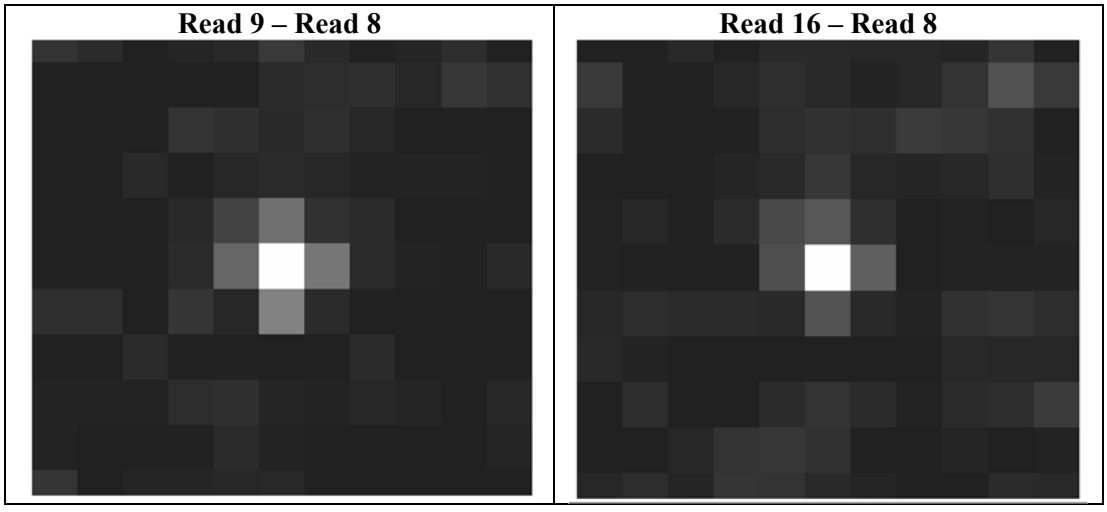

Figure 14: Combined averages of the 63 MeV sample hits from Picture 2

Table 8: Pixel Values Surrounding the hit pixel from the read immediately seconds after the hit at 63MeV, Picture 2. σ =0.014					
	1	2	3	4	5
1	0.001	0.004	0.005	0.003	0.001
2	0.005	0.018	0.040	0.009	0.005
3	0.006	0.035	1.000	0.044	0.006
4	0.010	0.004	0.049	0.005	-0.006
5	-0.004	-0.010	0.001	-0.001	0.005

Table 9: Pixel Values Surrounding the hit pixel from the read 42 seconds after the hit at 63MeV. σ = 0.019					
	1	2	3	4	5
1	0.003	0.005	0.012	0.003	0.002
2	0.006	0.021	0.028	0.008	-0.002
3	-0.005	0.023	1.000	0.032	-0.004
4	0.006	0.004	0.025	0.004	0.001
5	0.000	0.000	-0.004	-0.007	-0.002

Table 10: Sample Pixel Hits from Picture 3, 63 MeV							
Number	Pixel	read 9 – read 8 (e-)	read 16 – read 8 (e-)	Slope Before (e-/sec)	Slope after (e-/sec)	No hit before (e-/sec)	No hit after (e-/sec)
1*	(432, 506)	11043	12848	11.73	65.13	-0.76±1.33	0.53±0.98
2	(149, 117)	15521	15294	-4.55	2.19	0.16±0.79	-0.03±0.33
3	(200, 117)	7747	7873	11.90	1.19	0.29±1.73	0.43±0.75
4	(129, 270)	14338	14580	-5.96	4.54	-0.08±1.04	0.45±0.45
5	(239, 458)	35214	35478	-0.25	9.71	0.07±0.64	-0.03±0.45
6	(337, 456)	35520	35494	9.56	-4.84	-1.29±0.90	0.41±0.85
7	(373, 710)	30692	30552	-3.72	-4.62	0.13±0.48	-0.10±0.46
8	(289, 683)	12196	11928	2.69	0.066	0.05±1.02	0.19±0.71
9	(651, 774)	16486	16471	3.71	-4.70	-0.31±1.61	0.03±0.32
10	(564, 746)	31400	31470	-19.1	-9.24	-0.02±0.91	0.44±0.42
11	(474, 673)	19116	19264	14.69	14.08	0.22±0.76	0.18±0.82
12	(859, 688)	16704	16371	-12.91	-0.79	-0.56±0.84	0.24±0.50
13	(859, 638)	13885	13805	4.19	0.40	-0.05±0.52	1.10±0.98
14	(775, 283)	18692	18406	5.09	2.97	0.25±1.27	-0.07±0.96

*This pixel received a second hit and was removed from subsequent analysis.

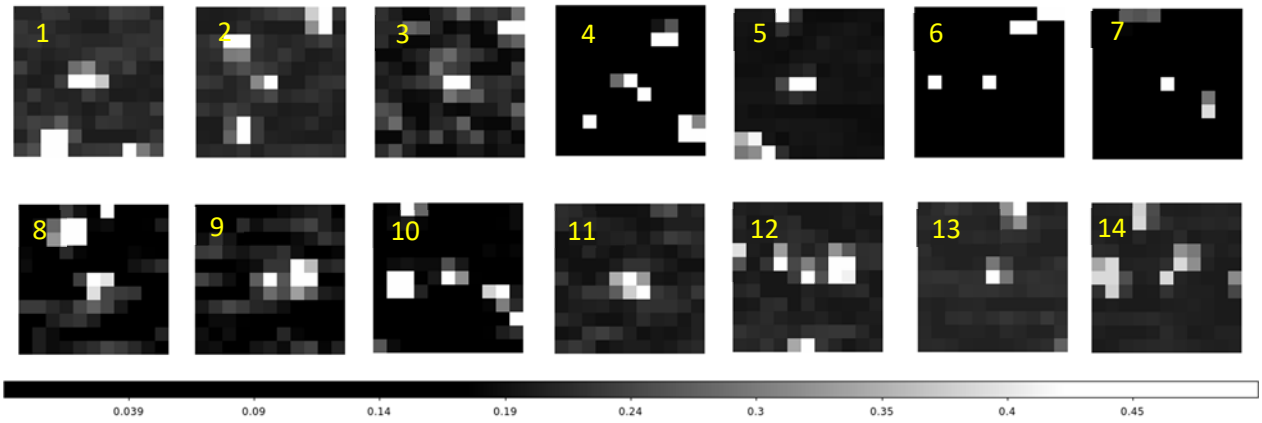

Figure 15: Grayscale images of the 14 hits in the 63 MeV sample from Picture 3, read 9 – read 8.

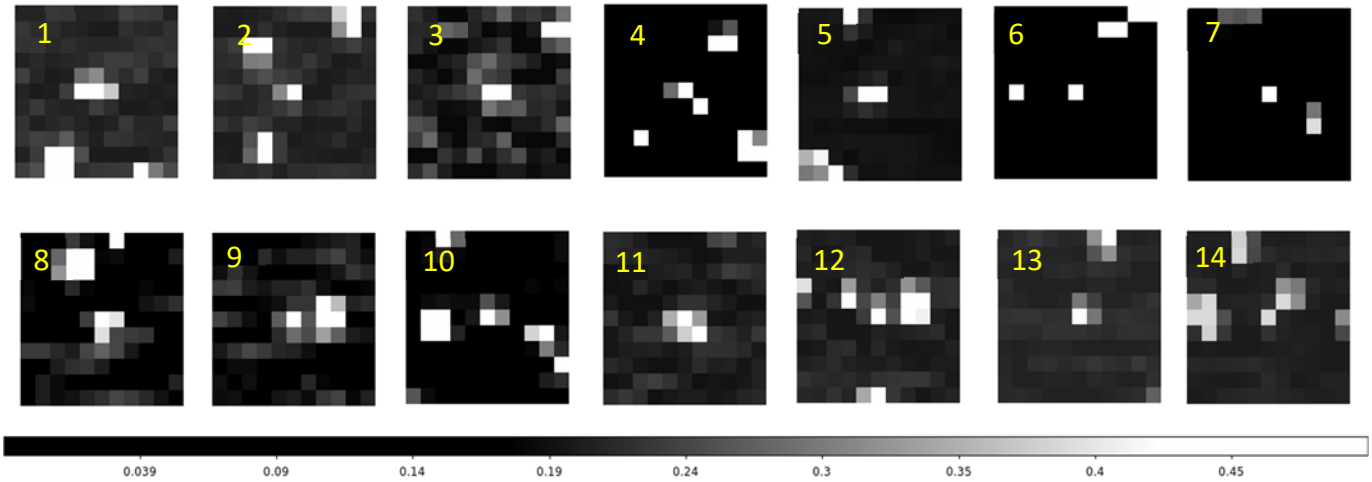

Figure 16: Grayscale images of the 14 hits in the 63 MeV sample from Picture 3, read 16 – read 8.

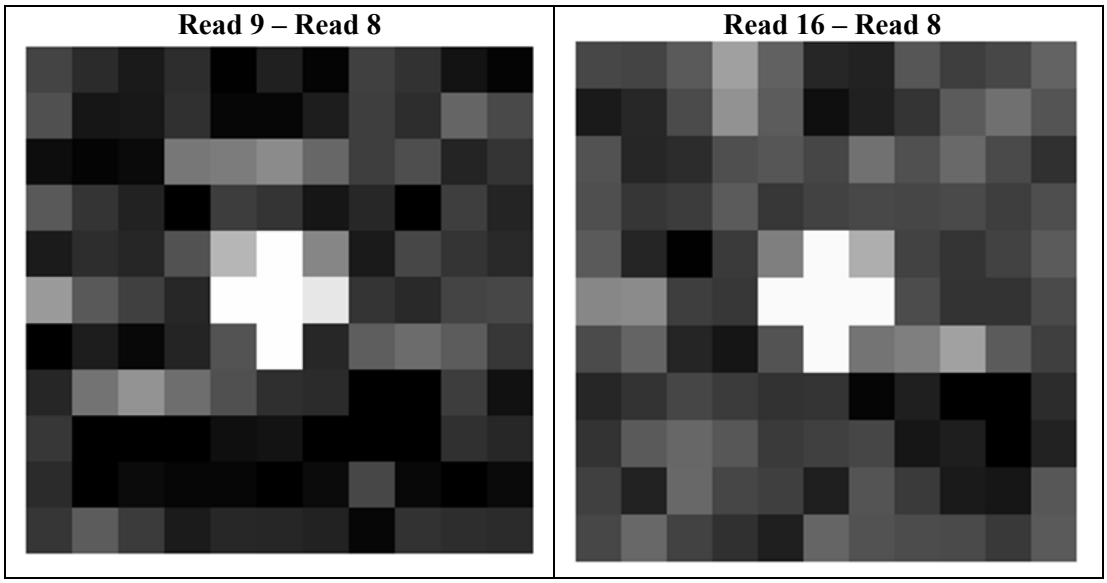

Figure 17: Combined averages of the 63 MeV sample hits from Picture 3.

Table 11: Pixel Values Surrounding the hit pixel from the read immediately seconds after the hit at 63MeV, Picture 3. $\sigma = 0.010$

	1	2	3	4	5
1	-0.005	0.003	0.002	-0.001	0.000
2	0.005	0.015	0.035	0.010	-0.001
3	0.000	0.049	1.000	0.020	0.002
4	0.000	0.005	0.035	0.0004	0.006
5	0.008	0.004	0.001	0.001	-0.010

Table 12: Pixel Values Surrounding the hit pixel from the read 42 seconds after the hit at 63MeV, Picture 3. σ =0.016					
	1	2	3	4	5
1	0.009	0.004	0.005	0.007	0.006
2	0.004	0.014	0.042	0.022	0.006
3	0.004	0.053	1.000	0.073	0.007
4	-0.001	0.008	0.043	0.013	0.014
5	0.005	0.003	0.004	-0.003	0.001

3.2 POST-HIT BEHAVIOR

3.2.1 Dark Current

Elevated dark current and an increase in the number of pixels with very high dark current (hot pixels) are the expected primary effects of proton irradiation. The 2002 radiation testing of an earlier generation of H2RG JWST-like arrays revealed these effects with very little change in the sensitivity to light. The ramps used to derive the dark current values in this test series were quite short with reset effects and similar issues likely dominating over real dark current in the quiescent state. Nonetheless, these results show that the higher energy irradiation induced an elevated dark current which decayed very quickly as described below. Dark ramps were analyzed by using linear fits as described in Section 2.1.1. The medians of the slopes from all 16-read images are shown in Figure 18. The median dark current returns to pre-exposure values quite rapidly. Figure 19 and Figure 20 show values near the proton exposure times.

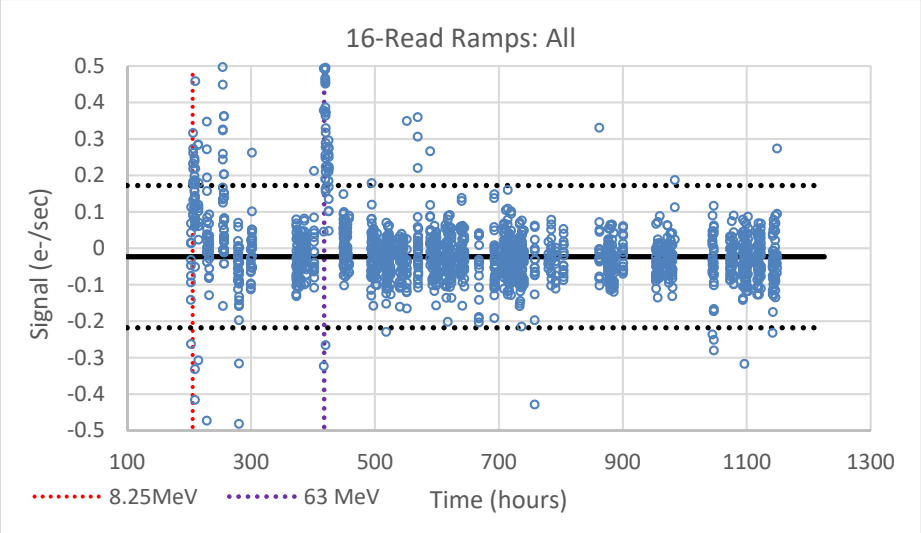

Figure 18: The dark current as measured from 16-read ramps for the entire cryogenic time span. The black dotted horizontal lines show plus and minus one sigma from the pre-exposure median.

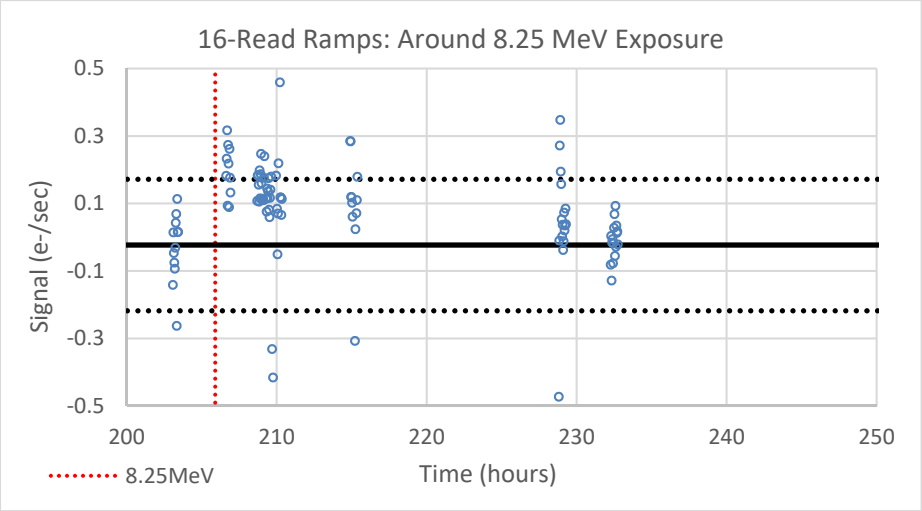

Figure 19: Portion of Figure 18 around the 8.25-MeV exposure.

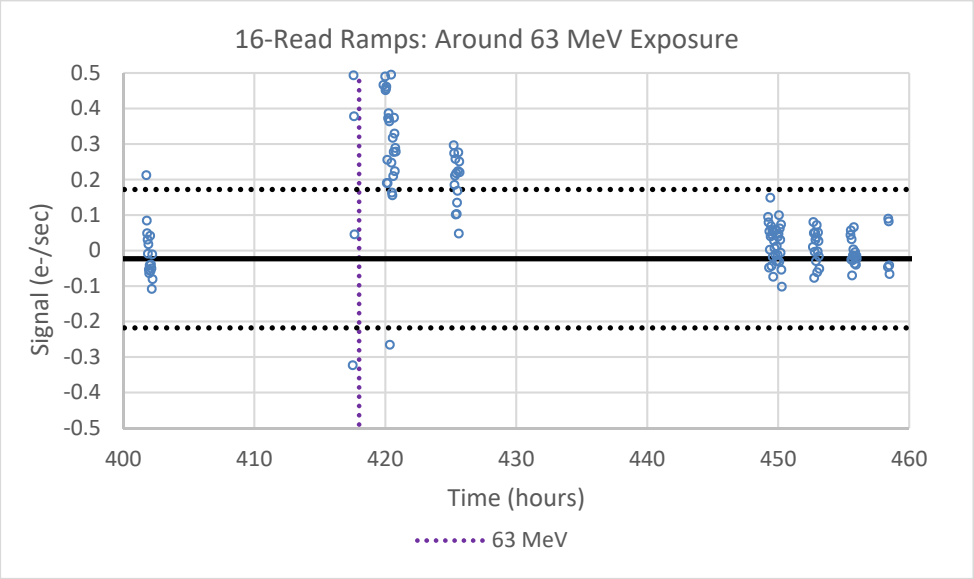

Figure 20: Portion of Figure 18 around the 63 MeV exposure.

The data taken using only 8 reads per ramps were analyzed in the same fashion as the 16-read ramps. Figure 21, Figure 22, and Figure 23 present the 8-read slopes.

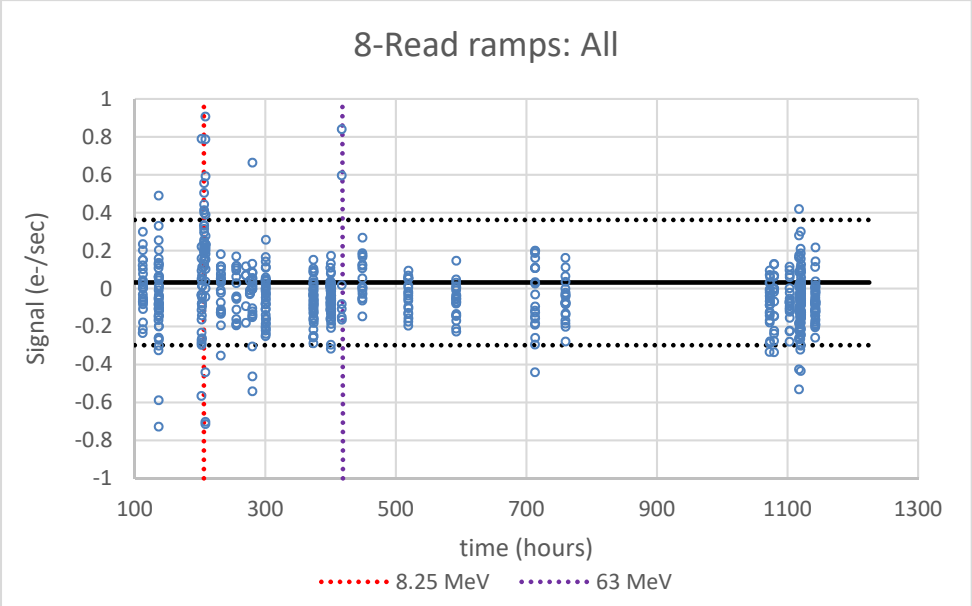

Figure 21: This figure presents all slopes from 8-read ramps in the same manner as Figure 18.

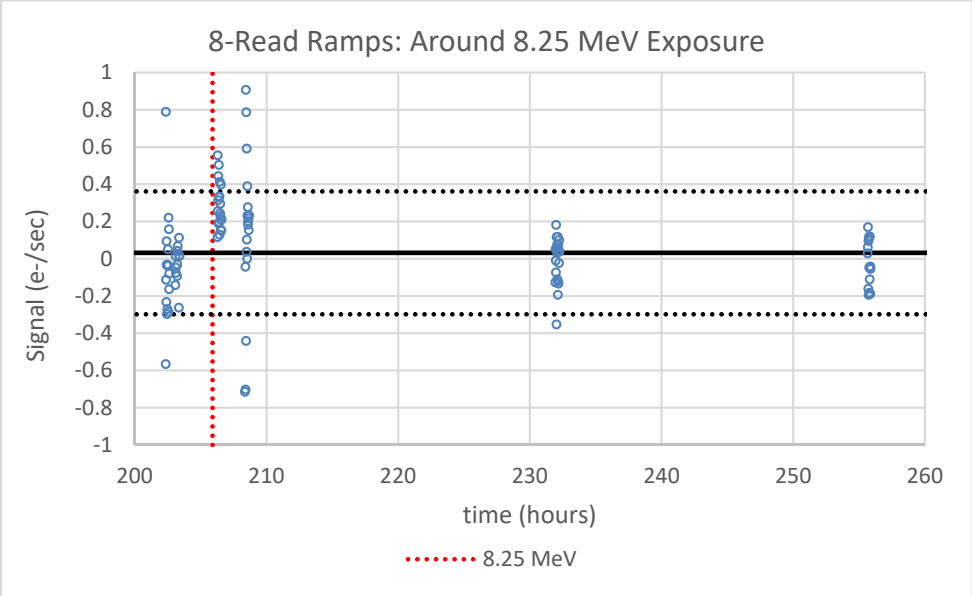

Figure 22: The 8-read ramp data around the 8.25 MeV exposure.

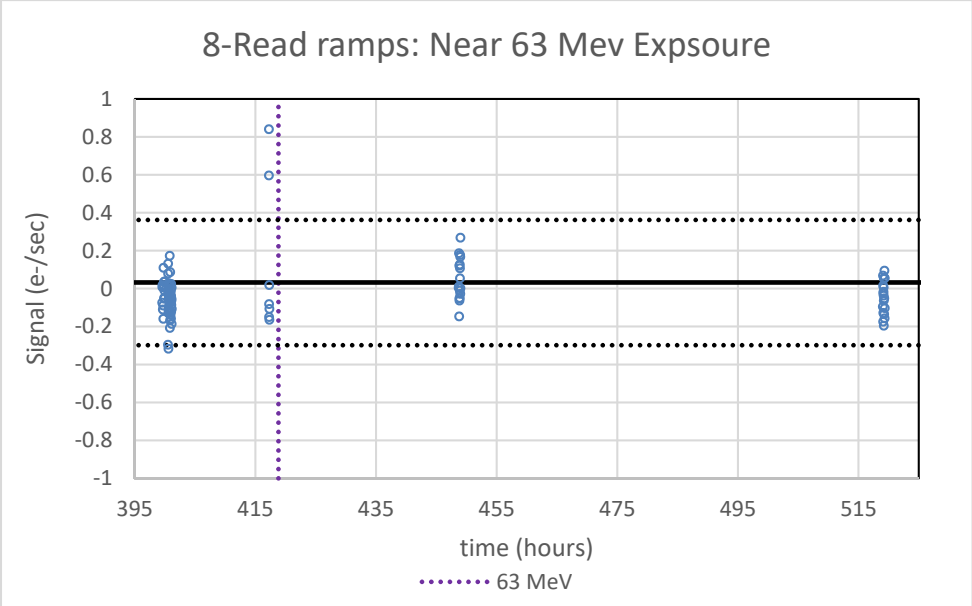

Figure 23: The 8-read ramp data around the 63 MeV exposure.

The median values are useful for looking at the behavior of the majority of the pixels, but are not useful for checking whether radiation exposure causes an increase in the number of high dark current or "hot" pixels. To look for such changes, histograms and the spread in distributions of pixel values in dark images are examined. Figure 24 and Table 13 show that the pixel distributions return to close to pre-exposure values within hours of the 8.25 MeV doses. The column labelled "No. of hits / read" in the table is an indication of how far the induced radioactivity in the dewar/array had decayed at the time of these dark current measurements. Subsequent figures and tables show the data taken in conjunction with the 63 MeV exposure and throughout the remainder of the test after the dewar was returned to Ames. The 63 MeV exposure took much longer to decay than the 8.25 MeV exposure. Note that it is difficult to distinguish between what might be dubbed "elevated dark current" and "persistence" due to the large amount of deposited charge in these proton exposures.

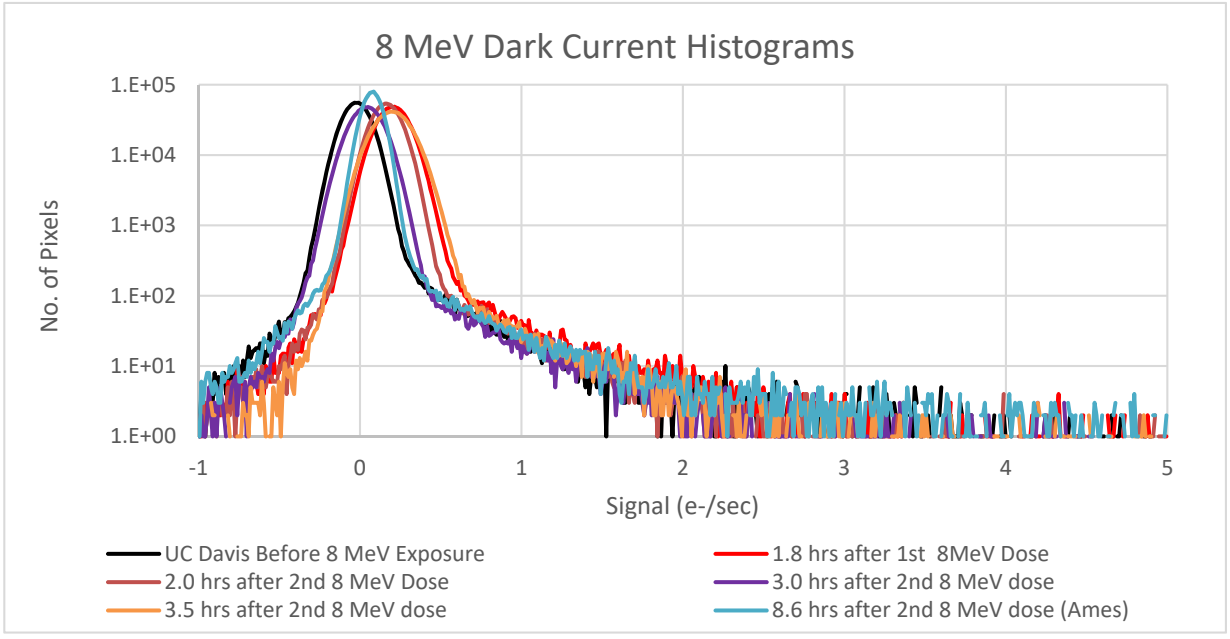

Figure 24: Dark current histograms before and shortly after the 8.25 MeV exposures.

Table 13: Median and standard deviations for histograms in Figure 24			
Run	No. of hits/read	Median Idk (e-/sec)	Std dev (e-/sec)
37K_3 before 8 MeV	738	-0.023	0.19
37K_10 1.8 hrs after 1st dose	698	0.202	0.19
37K_15 2.0 hrs after 2nd dose	123	0.161	0.22
37K_16 3.0 hrs after 2nd dose	119	0.037	0.36
37K_17 3.5 hrs after 2nd dose	121	0.195	0.56
37K_18 8.6 hrs after 2nd dose (Ames)	25.9	0.074	0.36

Table 14: Median and standard deviations for histograms in Figure 25			
Run	No. of hits/read	Median Idk (e-/sec)	Std dev (e-/sec)
37K_8 1.1 hrs after 1st 63MeV Dose	1847	0.568	1.68
37K_9 1.7 hrs after 1st 63MeV Dose	1207	0.432	1.16
37K_10 2.2 hrs after 1st 63MeV Dose	955	0.257	0.46
37K_16 1.3 hrs after 2nd 63MeV Dose	2039	0.663	4.47
37K_17 1.8 hrs after 2nd 63MeV Dose	1467	0.397	1.52
37K_18 2.3 hrs after 2nd 63MeV Dose	1198	0.301	0.83
37K_4 26.4 hrs after 2nd 63MeV Dose (2-19-2015)	149	0.036	0.13

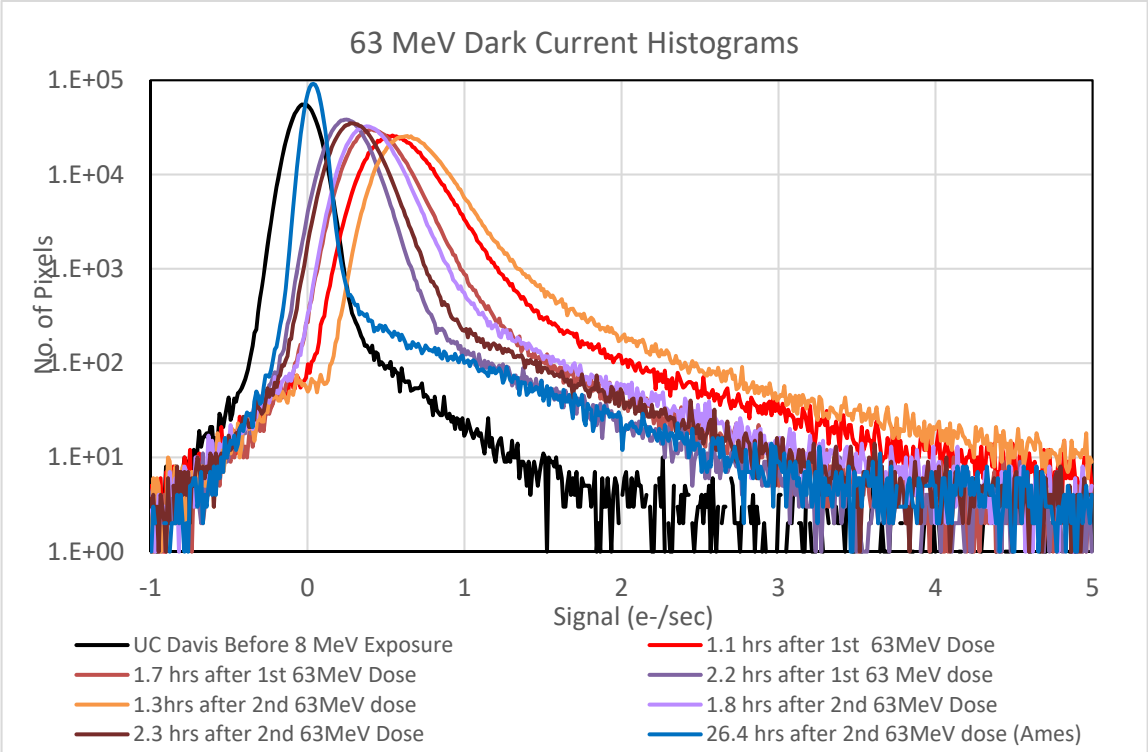

Figure 25: Dark current distributions before and shortly after the 63 MeV exposures.

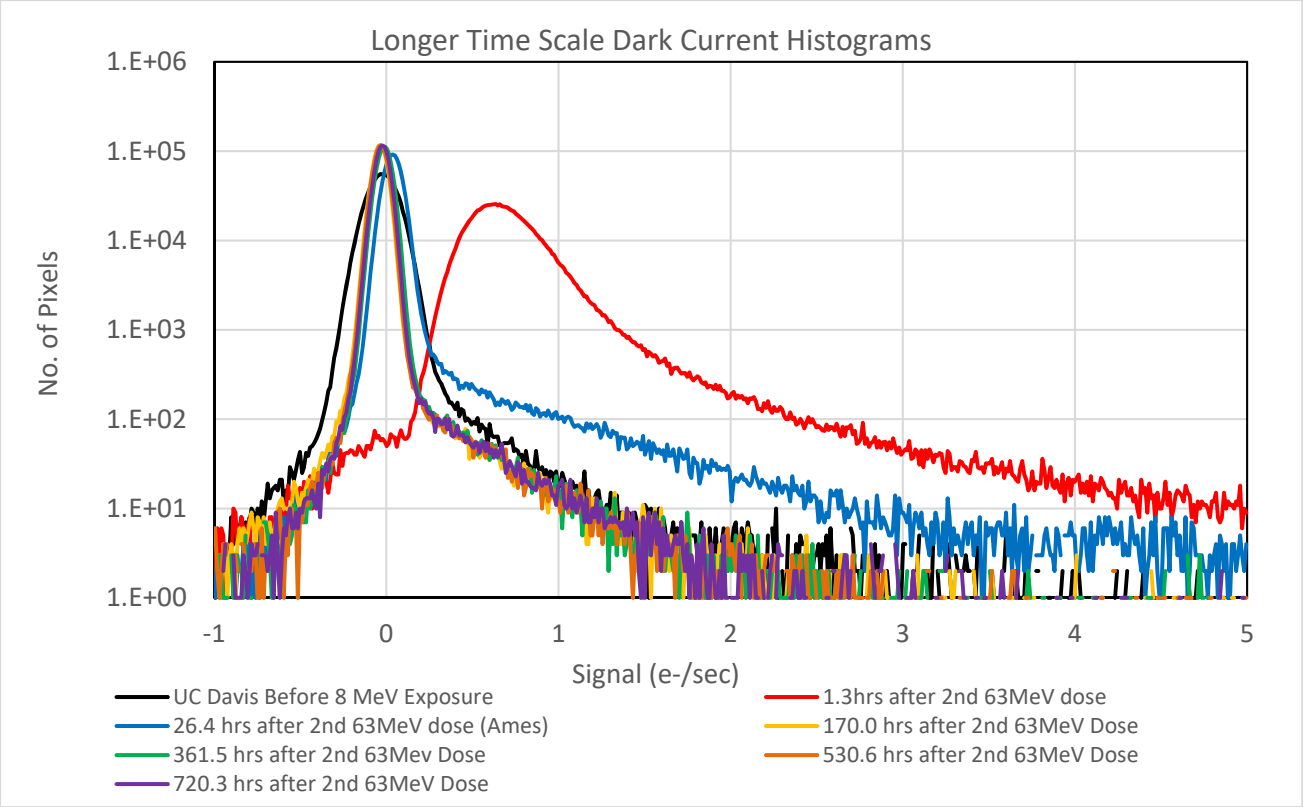

Figure 26: Dark current histograms long after exposure.

Table 15: Median and standard deviations for histograms in Figure 26			
Run	No. of hits/read	Median Idk (e-/sec)	Std dev (e-/sec)
Feb 18 37K_16 1.3 hrs after 2nd 63MeV Dose	2039	0.663	4.47
Feb 19 37K_4 26.4 hrs after 2nd 63MeV Dose	149	0.036	0.131
Feb 25 37K_21 170.0 hrs after 2nd 63MeV Dose	215	-0.039	0.098
Mar 05 37K_41 361.5 hrs after 2nd 63MeV Dose	78.8	-0.013	0.107
Mar 12 37K_46 530.6 hrs after 2nd 63MeV Dose	47.5	-0.035	0.099
Mar 20 37K_68 720.3 hrs after 2nd 63MeV Dose	37.5	-0.025	0.109

Another dark current comparison comes from data taken at Arizona before and after the radiation testing using the Arizona GL dewar test station. The read floor for these data, 6 e-, is much lower than for the data taken in the Ames dewar The one shortcoming of these data is that the array was warmed to ambient after the radiation test before the post-test dark current was measured. There were 204 days between the post-radiation exposure warm-up on March 20, 2015, and these data taken on October 10, 2015. There were 234 days since the last exposure to protons on February 18, 2015. This long period at ambient means that the higher dark current pixels observed in the October test are pixels which are permanently degraded, but not indicative of how many might be degraded due to radiation without this annealing period. The Arizona testing is more sensitive and able to measure very low dark currents as 1692-sec ramps were used to produce the histograms shown in Figure 8 and Figure 9. Appendix B describes the measurement procedure. Immediately apparent in these figures is that the median dark current did not change at all. The post-radiation exposure histogram does have a larger tail of pixels with elevated dark current. The increase in the number of pixels with $I_{dk} > 0.05$ e-/sec after radiation exposure is 0.67% of the total number of good pixels before exposure in the full frame data. The

increase in the corner region is 0.71%. Table 16 lists the medians for these data.

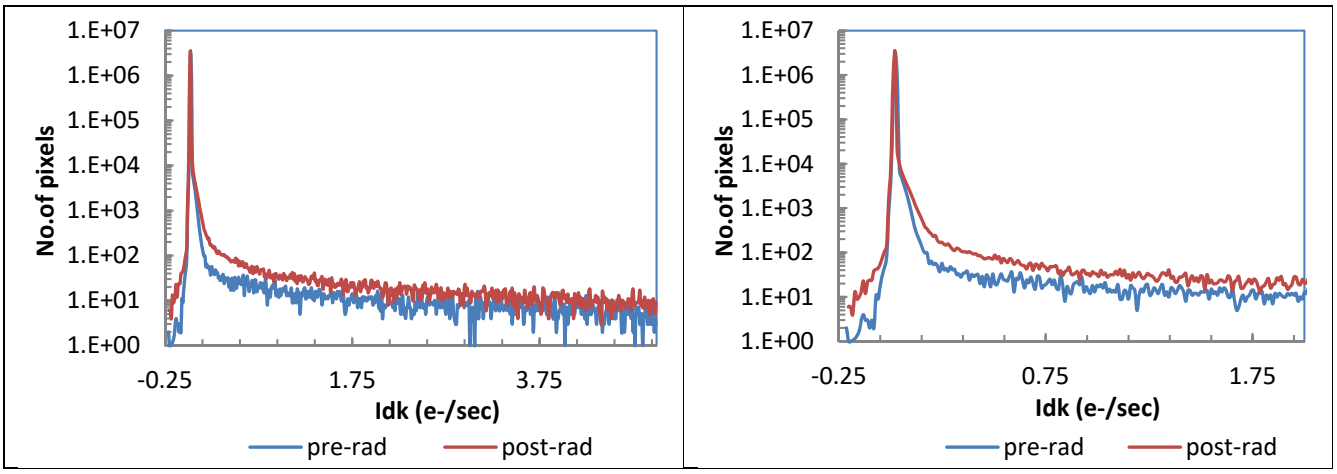

Figure 27: Histogram of dark currents as measured in 1692-sec ramps at Arizona at 39.5 K as derived from the full 2Kx2K pixels. The right hand panel presents a magnified version of the left hand panel.

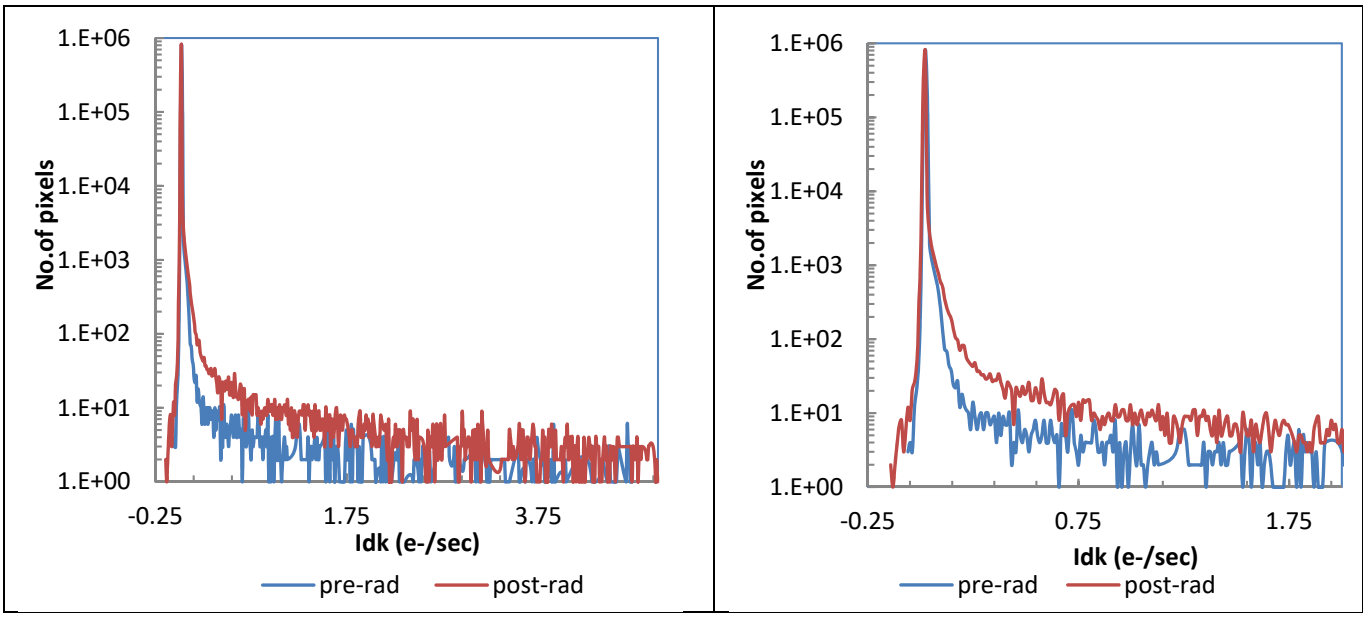

Figure 28: Dark current histograms for only the 1024x1024 region measured in the radiation testing. The right hand panel presents a magnified version of the left hand panel.

Table 16: Dark Current Statistics for Arizona Tests

Region	Median Idk e-/s pre-exposure	No. of pixels in pre median	Median Idk e-/s post-exposure	No. of pixels in post median
Full array	0.022	4159487	0.015	4157116
Corner	0.025	1039903	0.018	1039173

3.2.2 Persistence

Infrared detector suffer from an effect called latent images or persistence which is seen as "signal" in a pixel after charge has been accumulated in that pixel earlier. See Leisenring et al. 2016, Proceedings of the SPIE, Volume 9915, id. 99152N, for results on this effect due to charge generated by photons.

Figure 29 shows plots of the persistence signal from the array used in the radiation testing. The various curves result from differing levels of illumination where pixels were filled from roughly 10% of full well to over twice saturation. The persistence decays on two time scales – one time constant of ~200 seconds and one longer of ~1000 seconds. The persistence amplitude is proportional to the level of illumination and inversely proportional to the illumination rate such that charge deposited very rapidly produces much smaller persistence. The data in Figure 29 are array median values.

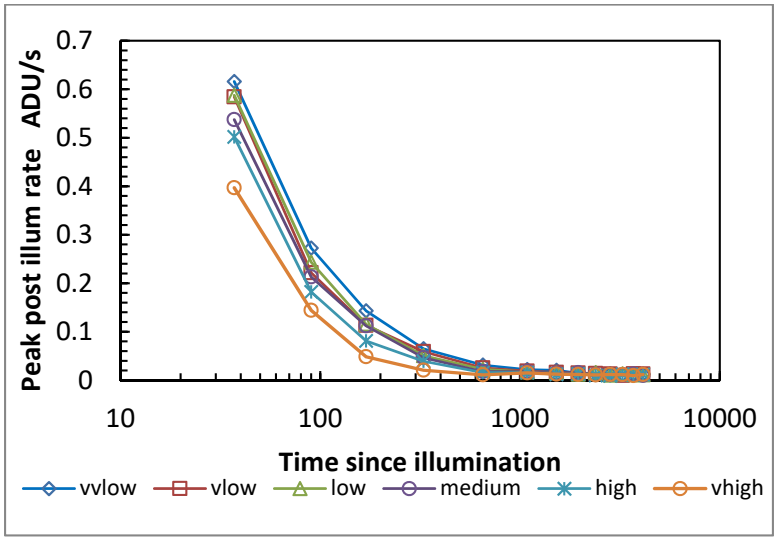

Figure 29: Decay of effect of illumination on pixels in the array 17159. Multiply ADUs/sec by 2.7 to convert to e-/sec.

To investigate whether charge deposition by charged particles produces the same type of persistence as charge deposition from illumination, post-hit reads of pixel hits examined in Section 3.1 were studied. The sprinkle data were used as the higher proton rates completely saturated all pixels, and the signal decay shown in Section 3.2.1 might be due to persistence, but the extremely high levels are not indicative of what effects single hits on-orbit will cause.

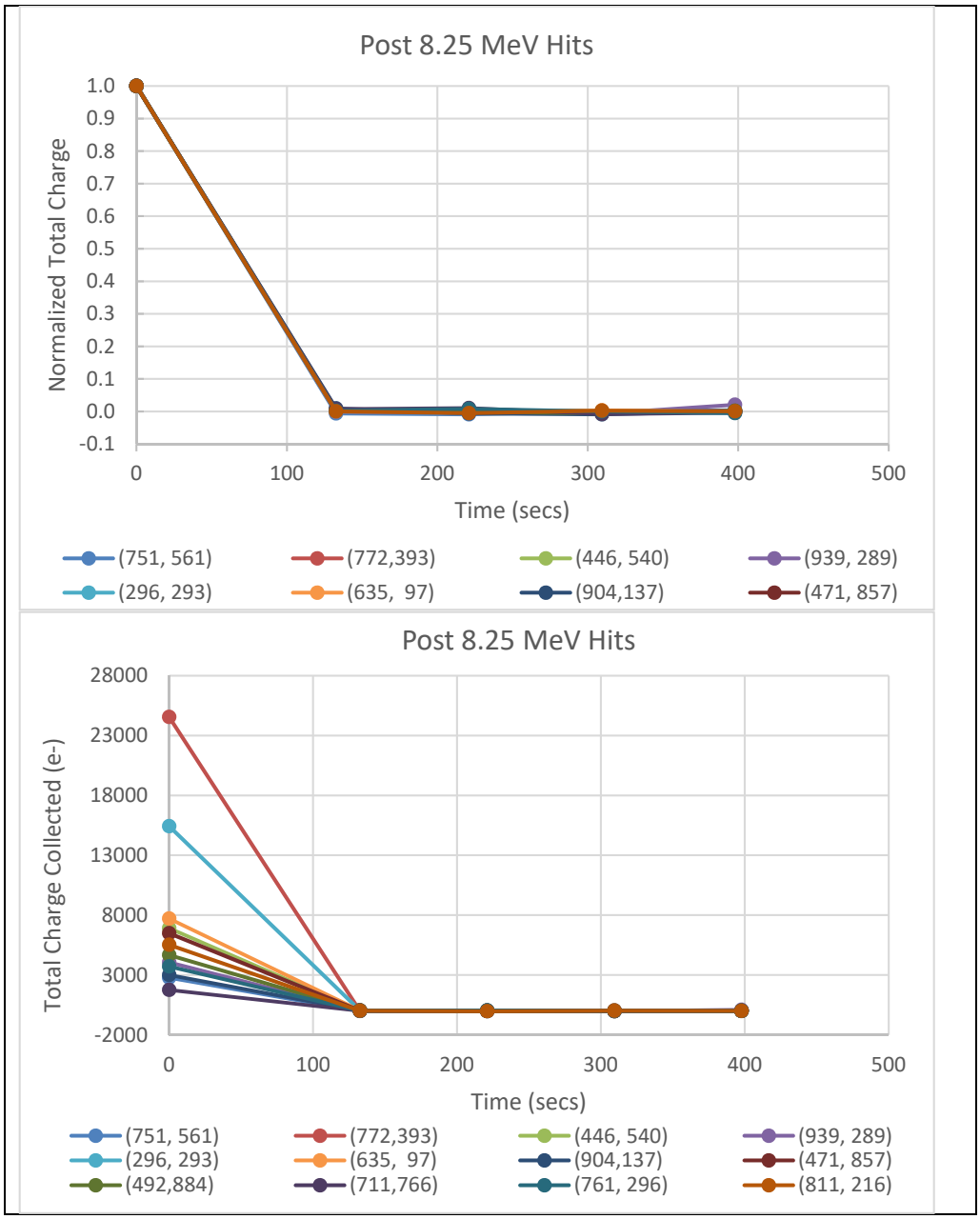

Figure 30: Single pixel hits and induced charges for a sample of pixels from the 8.25 MeV data. The top panel shows the total charge and subsequent charge collection in several ramps while the bottom panel normailizes all hits to unity.

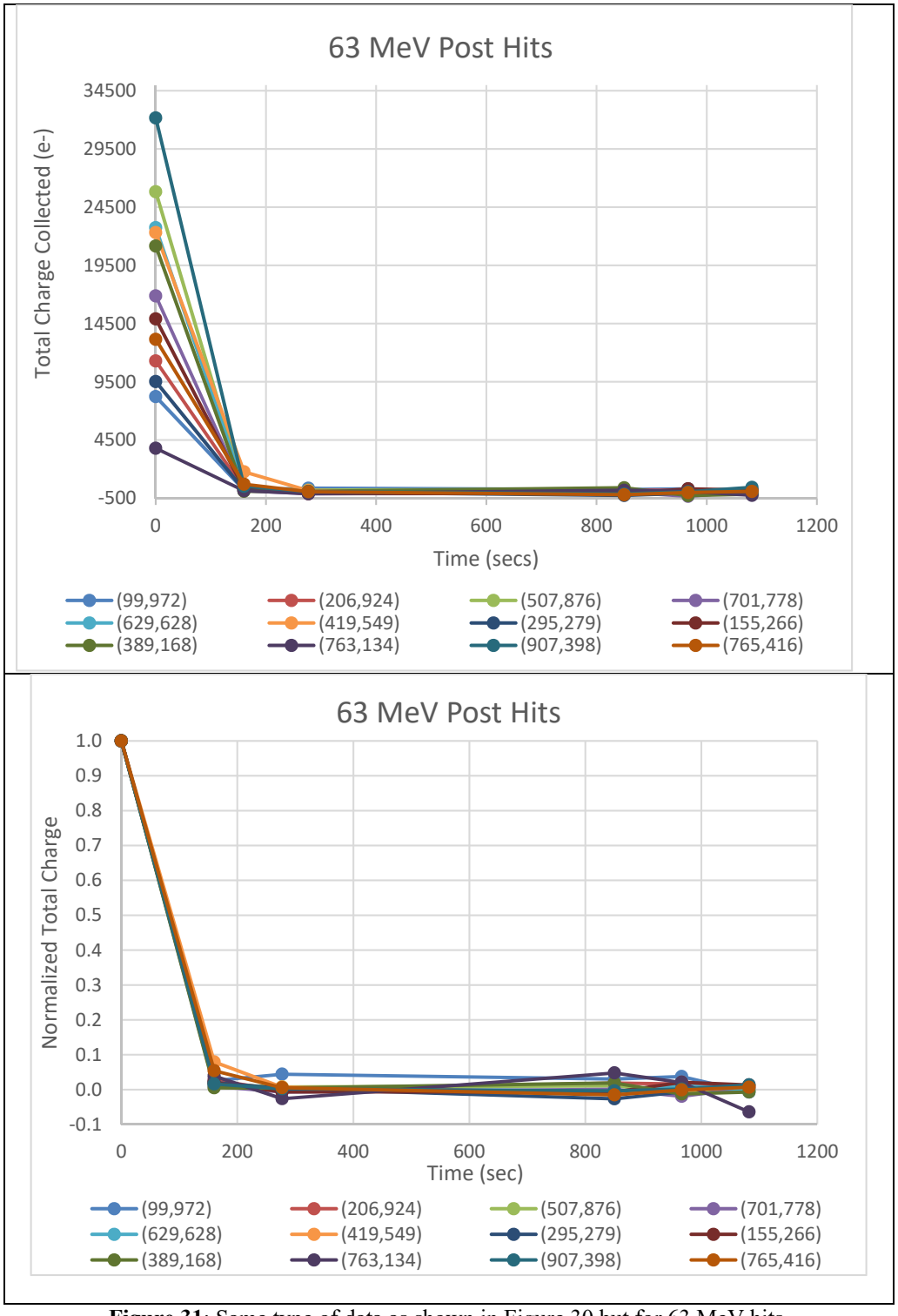

Figure 31: Same type of data as shown in Figure 30 but for 63 MeV hits.

These data suggest that cosmic-ray hits on orbit will produce effects similar to charge collection from illumination, but the noise floor of the Ames system prevents stronger conclusions from being drawn.

3.3 ILLUMINATED TESTING USING DEWAR LED

The Ames test dewar is equipped with a 0.95 micron LED that was used to track response to light. Figure 32 shows the illumination pattern, and the fact that little change was apparent due to the 8.25 MeV exposure. However, Figure 33 shows that the 63 MeV exposure may have caused a change in response. The large spread in response values seen several times such as at 255 hours and 712 hours are likely due to instability in the LED output as discussed below.

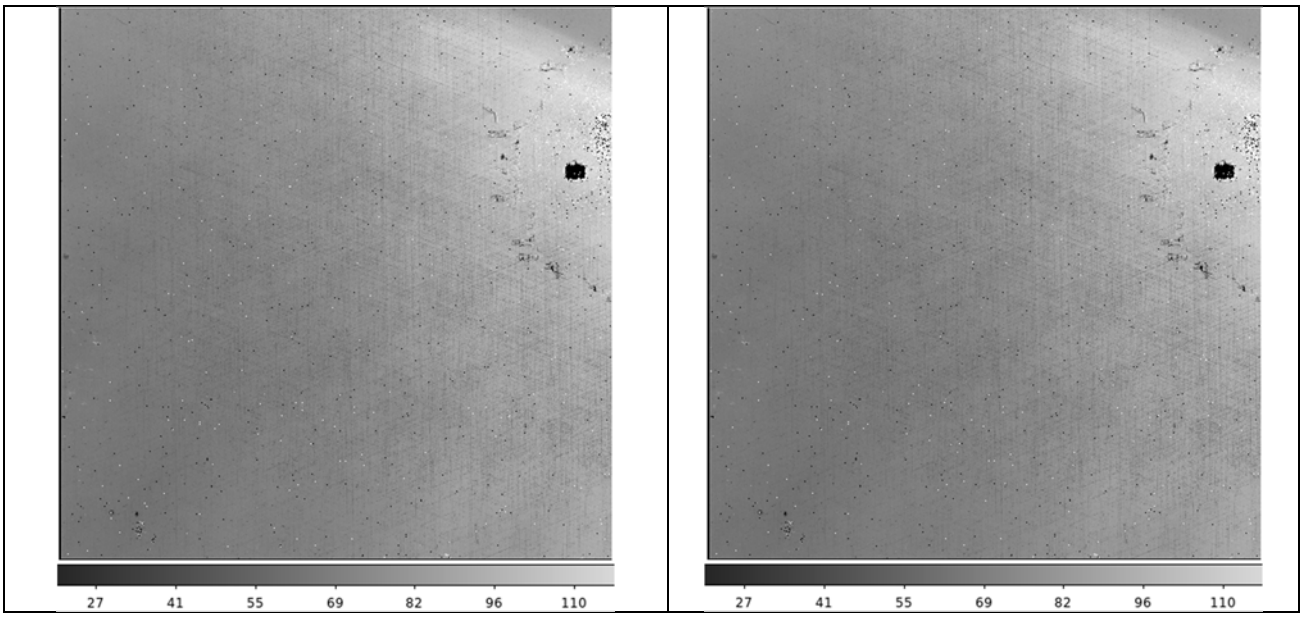

Figure 32: The illumination pattern produced by the dewar LED. The left panel is before any exposure to protons and the right panel is immediately after exposure to 8.25 MeV protons. The grayscale units are e-/sec.

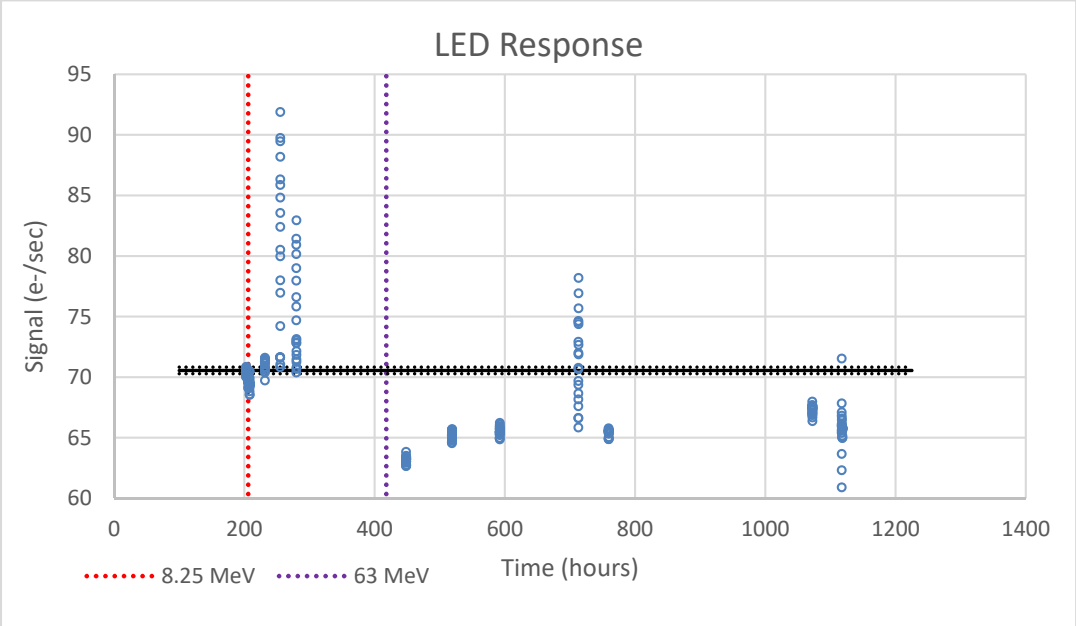

Figure 33: LED signals over the entire test period.

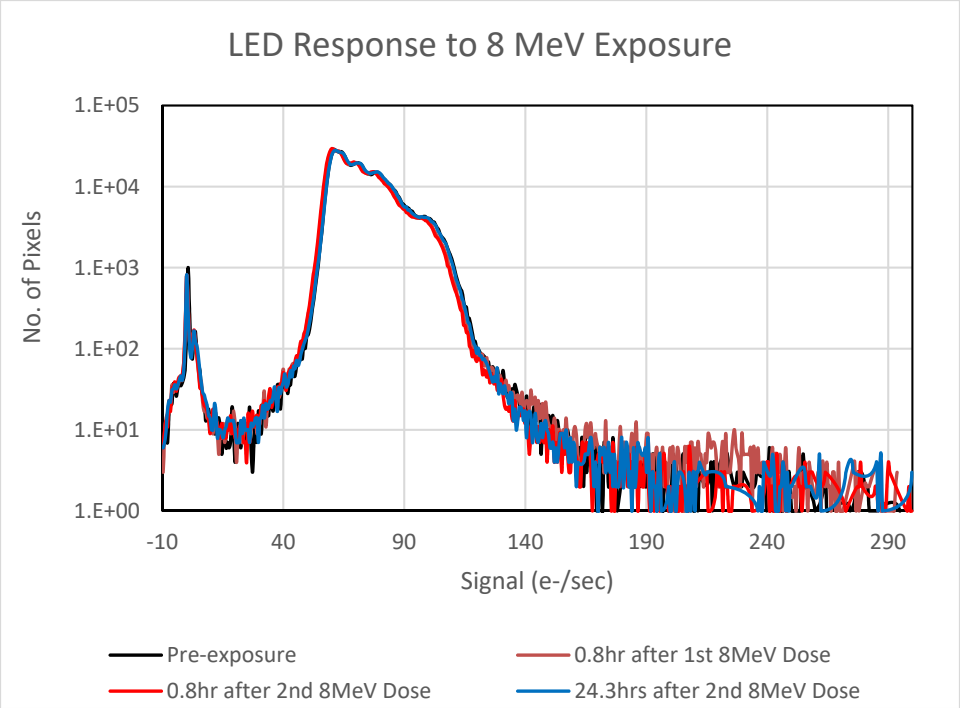

Figure 34: Histograms of the pixel signal slopes before and after irradiation at 8.25 MeV.

The histograms in Figure 34 confirm the lack of change due to proton irradiation. Table 17 lists the medians which do not vary outside the bounds effected from counting statistics.

Table 17: Medians and standard devistions for the histograms in Figure 34.

Run	slope	sigma
Feb 9 37K-2 Pre-exposure	70.5	1.69
Feb 9 37K_8 0.8hr after 1st 8MeV Dose	69.8	1.53
Feb 9 37K_13 0.8hr after 2nd 8MeV Dose	69.5	1.58
Feb 10 37K_2 24.3 hr after 2nd 8MeV Dose	71.1	1.46

The histograms of the response at 63 MeV as shown in Figure 35 and medians listed in Table 18 suggest that the array lost ~10% of its sensitivity to light due the 63 MeV irradiation. The histograms in Figure 35 have very similar shapes which suggests that the change is in an element of the array common to all pixels. Since two output amplifiers are included in the array test area, one would expect to see a slight difference between the two stripes in the gray scale images in Figure 36 while none is seen. Other explanations would not produce such a uniform change in the histograms so a more likely explanation is that the output of the LED changed slightly which would affect all illuminated pixels the same way.

Figure 37 through Figure 39 present more detail for the large responses variations apparent in Figure 33. These variations are not plausibly due to the array itself, and suggest strongly that the LED output has some variability.

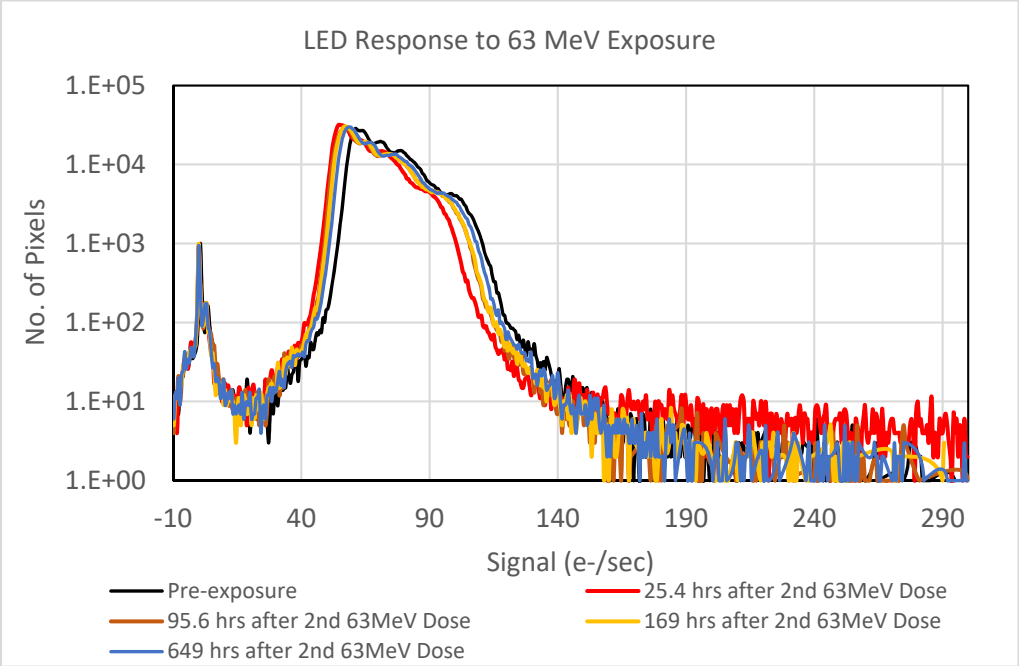

Figure 35: Histograms of LED response after the 63 MeV exposure.

Table 18: Medians and standard deviations for the histograms in Figure 35.

Run	slope	sigma
Feb 9 37K-2 Pre-exposure	70.5	1.69
Feb 19 37K_2 25.4 hrs after 2nd 63 MeV Dose	63.2	1.38
Feb 22 37K_10 95.6 hrs after 2nd 63 MeV Dose	65.5	1.42
Feb 25 37K_19 169 hrs after 2nd 63 MeV Dose	65.5	1.45
Mar 17 37K_53 649 hrs after 2nd 63 MeV Dose	67.3	1.43

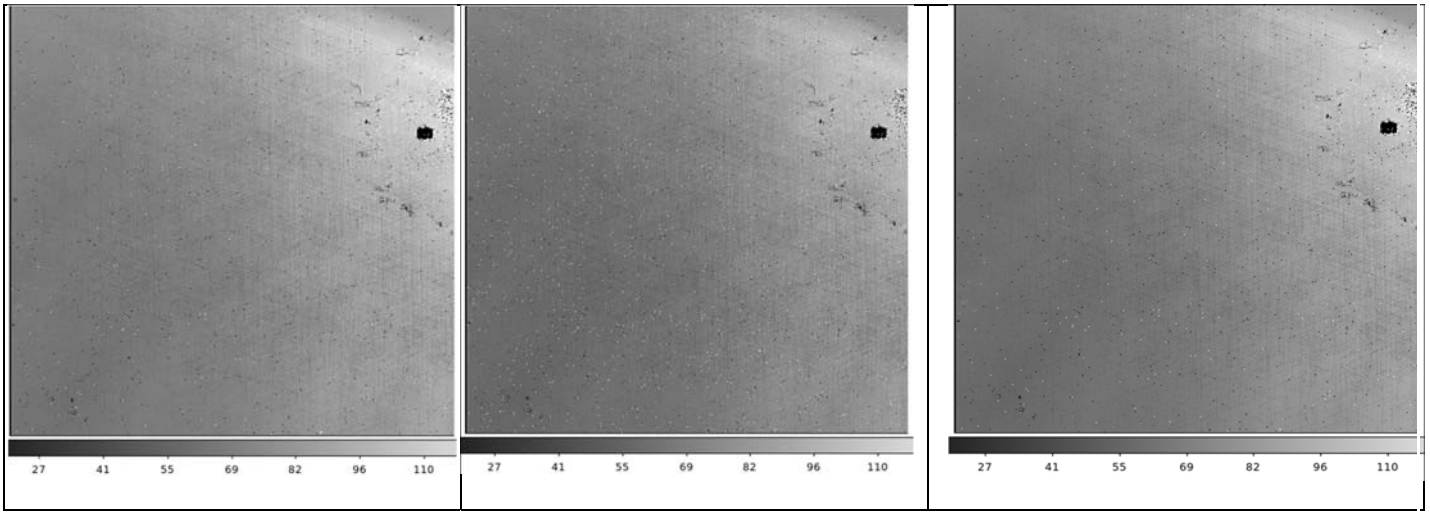

Figure 36: Grayscale representations of the LED response pre-exposure on the left, immediately after the 63 MeV exposure in the middle, and at the end of the entire test on the right. The grayscale units are e-/sec.

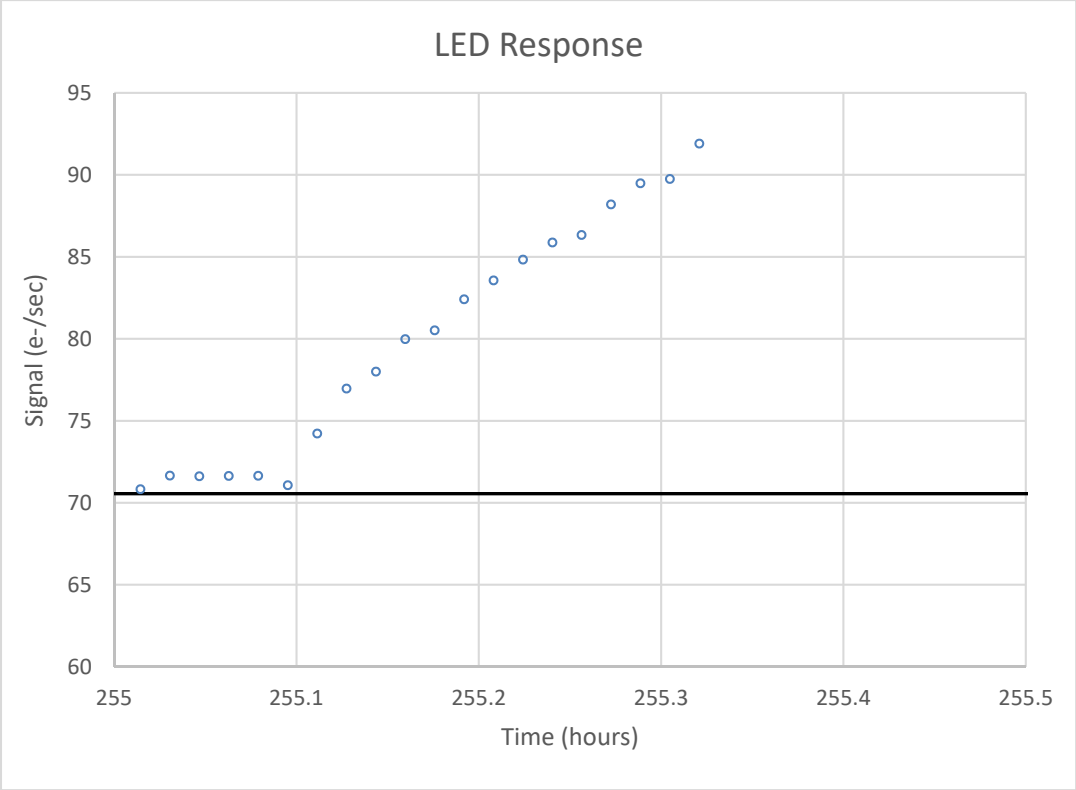

Figure 37: LED response variations near 255 hours showing the same signal level as pre-exposure followed by a gradual increase in signal. The black line and dotted lines show the pre-exposure level plus and minus one-sigma.

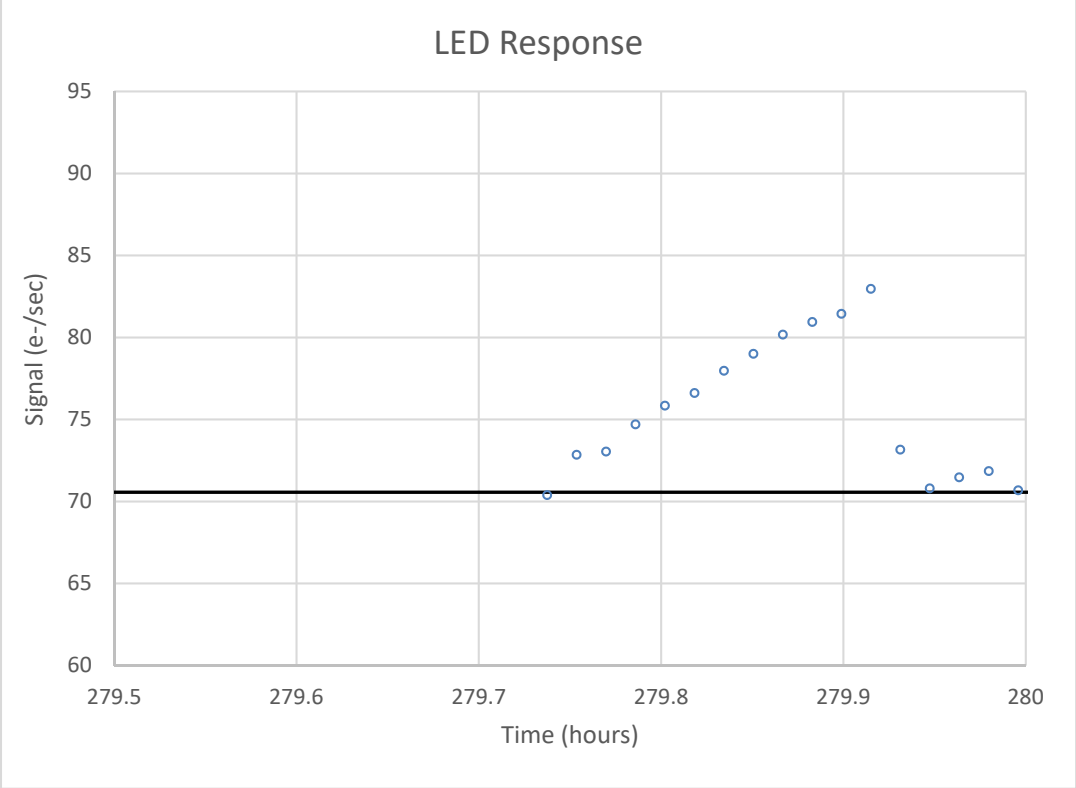

Figure 38: LED response variations near 280 hours presented in the same format as Figure 37.

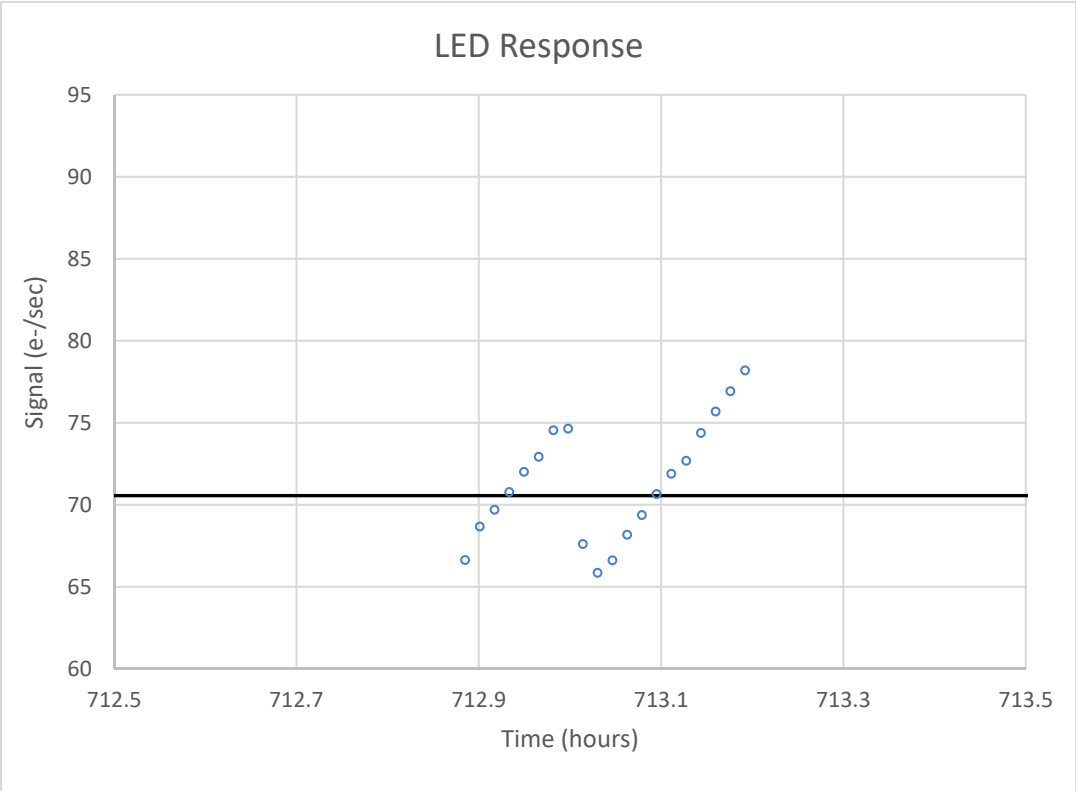

Figure 39: LED response variations near 712 hours presented in the same format as Figure 37.

3.4 TRANSFER FUNCTION

Radiation can cause shifts in the threshold voltages of transistors. The transfer function datasets were taken to look for such effects. If the threshold voltages changed in the readout for the H2RG, then there is a potential for different offsets in image data and possibly changes in the photometric calibration. Apparent levels at which saturation occurs could also change. The tests run as part of this program showed no shifts so the usual procedures for monitoring detector behavior should be adequate.

3.5 LINEARITY

Measuring the linearity of an H2RG array requires a stable light source and the ability to take long ramps. The ramps taken in the Ames dewar with its LED only reached a total charge collection of approximately 10% of full well. This level of charge collection does not probe the non-linear regime at all. Figure 40 shows Arizona test data where there is no difference between pre- and post-radiation behavior ut with the caveat that more than 200 days, mostly at room temperature, elapsed between the last proton exposure and the post-radiation measurement.

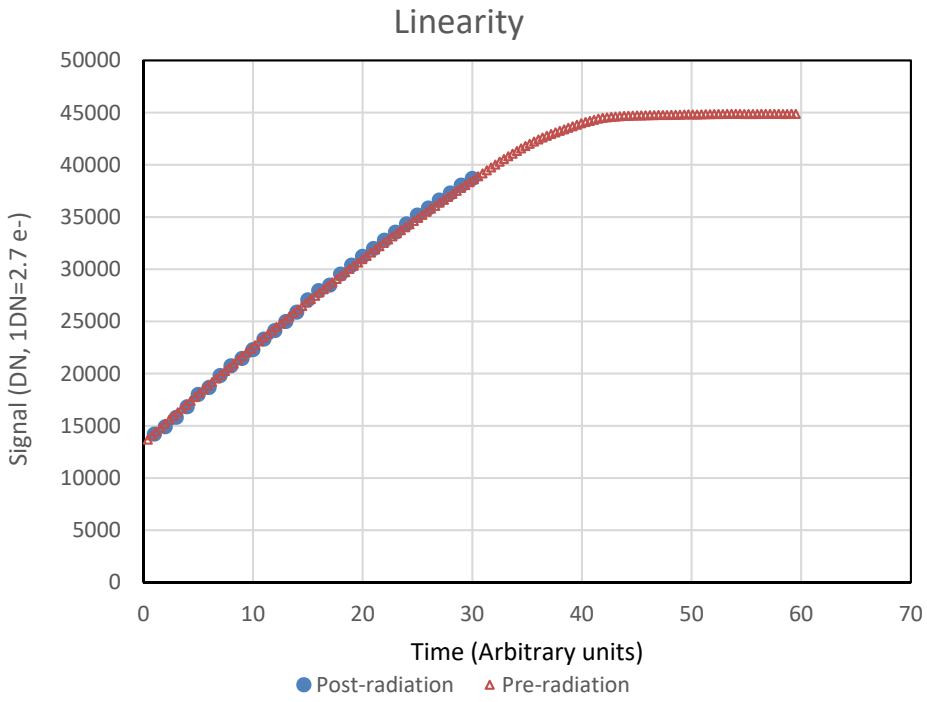

Figure 40: Linearity data from the Arizona test dewar. The array was not kept cold between irradiation the post-radiation data.

3.6 GAIN MEASUREMENT

The gain measurement technique used at Arizona follows the prescription of the signal variance method extrapolated back to zero signal (see JWST-REF-011321). The gain was measured before irradiation and post-irradiation in the Arizona test dewar but with the post measurement 200 days after irradiation, and with time spent at room temperature between irradiation and the gain measurement. No statistically significant difference in gain was observed. Figure 41 displays the gains for each pixel in a color-scale format with all 2040x2040 pixels shown. Figure 42 shows plots of gain versus signal strength with the reported gains being the extrapolation of these curves to zero-signal. Figure 43 shows the histograms of the gain values for all 2040x2040 pixels.

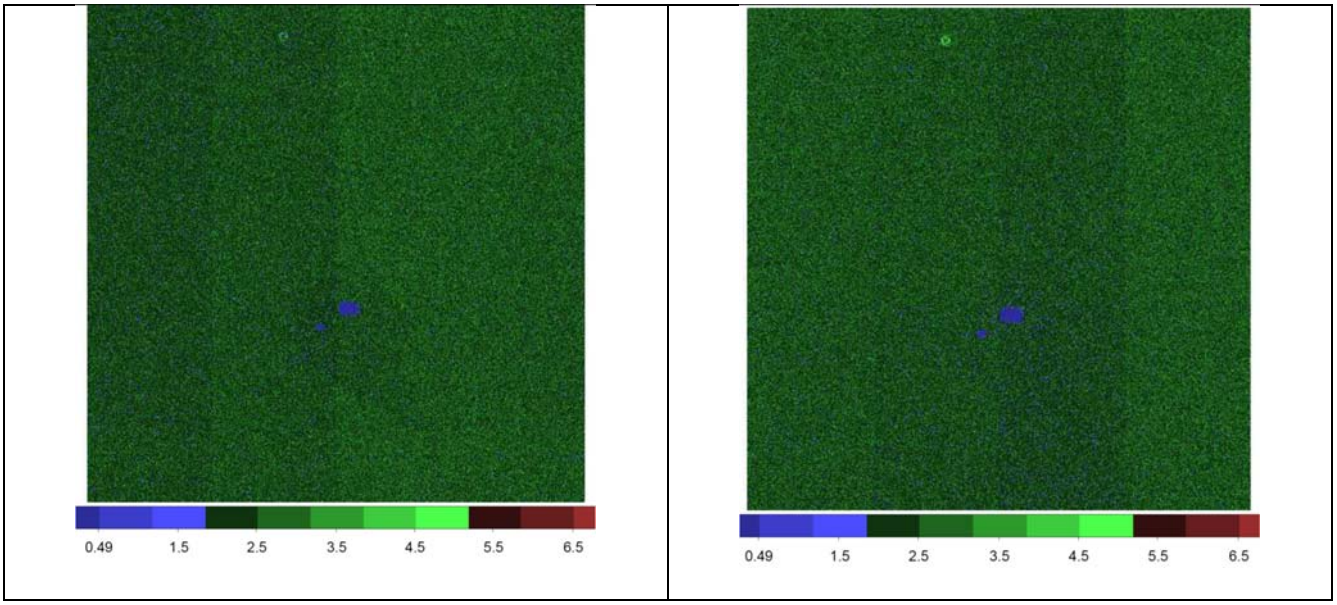

Figure 41: Left hand panel shows the gain measurement before proton exposure while the right hand panel show the post exposure result. The color bars are in units of e-/A-to-D units. The array was warmed to room temperature between pre- and post-exposure measurement.

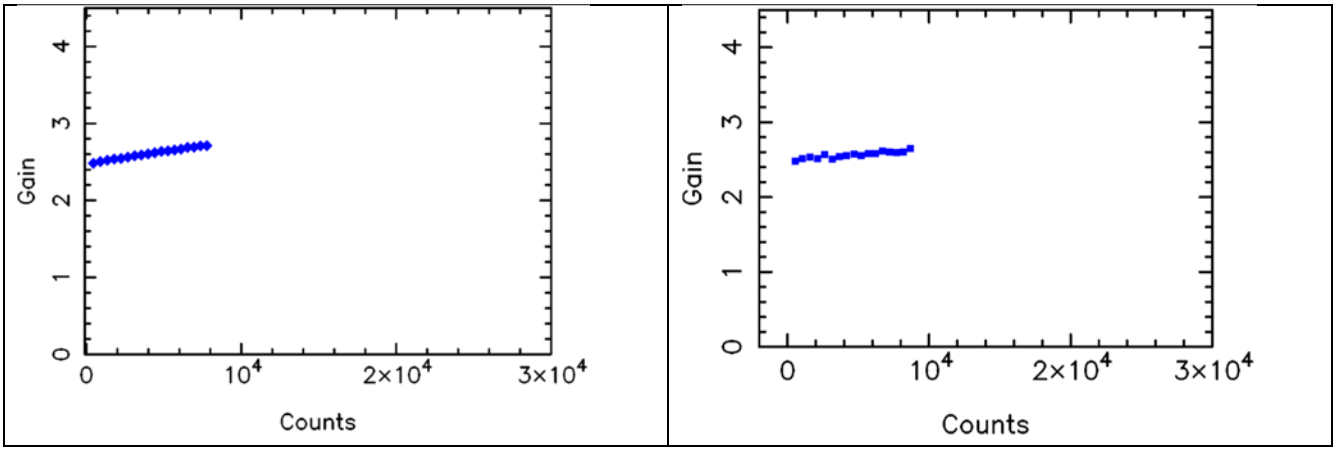

Figure 42: Plots of signal counts in analog-to-digital converter units versus gain, left hand is pre-exposure and right-hand is post.

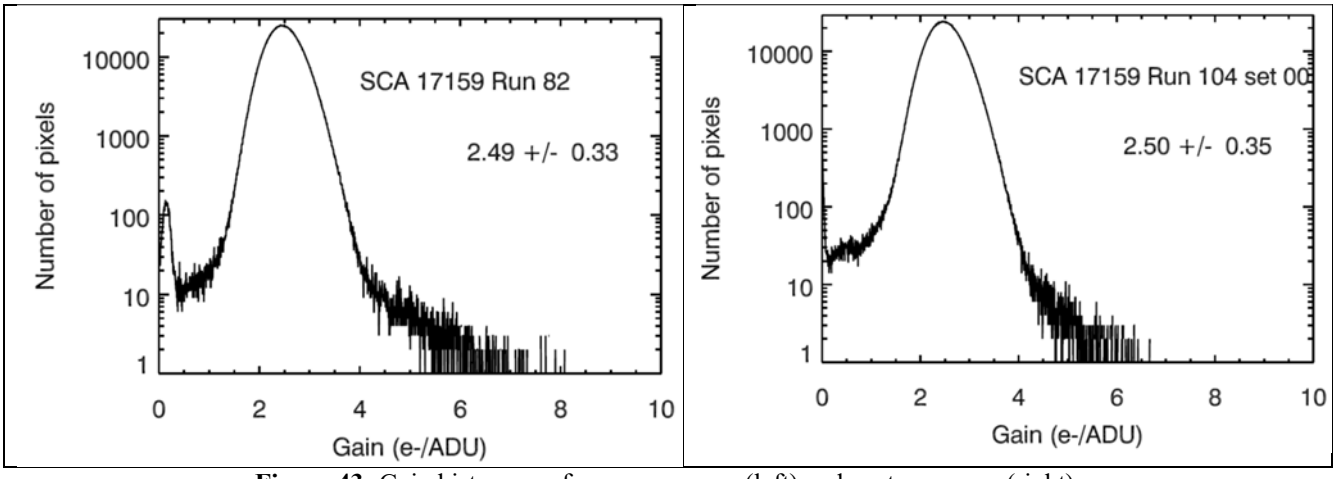

Figure 43: Gain histograms for pre-exposure (left) and post-exposure (right).

Appendix B. ARIZONA PROCEDURES FOR BASIC SCA CHARACTERIZATION

Performance of sensor chip assemblies (SCAs) intended for use in NIRCam was measured in a GL Scientific dewar with an internal dome that can be illuminated by a selection of LEDs and using Lakeshore controllers for temperature control, and Astronomical Research Cameras readout electronics. None of the Arizona results reported have been corrected for inter-pixel capacitance effects so they will be ~10% higher than Teledyne values.

Table 19: Summary of Arizona Test Dates

	Arizona Performance Tests	Dates	Data Collected
Test			
Pre-Rad	Run 81, Run 82	R82: 5/14/-5/29/2013	Run 81 darks only
Post-Rad 1	Run 014	10/08 - 27/2015	Darks, LED, Gain
Post-Rad 2	Run 107	03/08-03/12/2016	Darks, LED

Table 20: Summary of Arizona Measurements

QE 3.5/4.4um	CDS e-	RN e-	36.5K Idk e/s	39.5K Idk e/s	47K Idk e-/s	total well e-	"low" latent e-/s
0.82/0.84	14.9	8.4	0.029	0.029	0.032	89600	1.69

B1. Array Control

The array biases, clocking, and signal digitization are provided by an Astronomical Research Cameras Generation III controller ("Leach" controller) with two clocking boards and two video boards which permit simultaneous operation of up to four arrays. The shorted input correlated double sample noise for these tests was approximately 10 electrons, and the shorted input noise in a long ramp (90 reads spanning 954 seconds) is 6 electrons. These values are for the Leach system only, and have not been backed out of the results reported here. This array controller currently uses the buffered output mode of the H2RG, uses enhanced clocking mode, and uses pixel by pixel resets. The Leach and H2RG operating parameters are listed in Table 21 and Table 22. The biases used are listed in Table 3.

Table 21: H2RG Control Register Values

SCA Register	Value	Function
HoriRegDir	Default = 10101010	Horizontal readout directions: →←→←
GainReg	Default = 00010000	Not relevant for slow readout
OutputModeReg	Default = 01110010	Use 4-outputs, Window out output #7

OutputBufReg	Default = 00010001	Use buffered output, slow mode
NormalModeReg	00000011	Vertical scans bottom to top, enhanced clocking
WindowModeReg	00000011	Vertical scans bottom to top, horizontal scans left to right, enhanced clocking
MiscReg	00001100 (default) or 00001111	Full frame, one pixel per HCLK cycle Window mode, one pixel per HCLK cycle
PowerDownReg	Default = 01010101	Not relevant for slow mode
OptionsReg	Default = 0000	VCLK and FRAMESYNC can be used to control serial interface

VertStartReg, VertStopReg, HoriStartReg, HoriStopReg set to 0, 2047, 0, 2047 for full frame or to the start and end coordinates of window in window mode.

Table 22: Leach Electronics Parameters	
2.15 (Run18), 2.20 (Run50), 2.1 (Run 57)	Video offset Stripe 1
"	Stripe 2
"	Stripe 3
"	Stripe 4
2.500	DAC 0 = A/D Converter Gain
2.700	DAC 7 = Vsource

The Leach controller is run via a custom Linux program which can either operated from a GUI or from scripts. Most data are acquired using scripts to ensure uniformity, and some tests such as latents can only be acquired using a script.

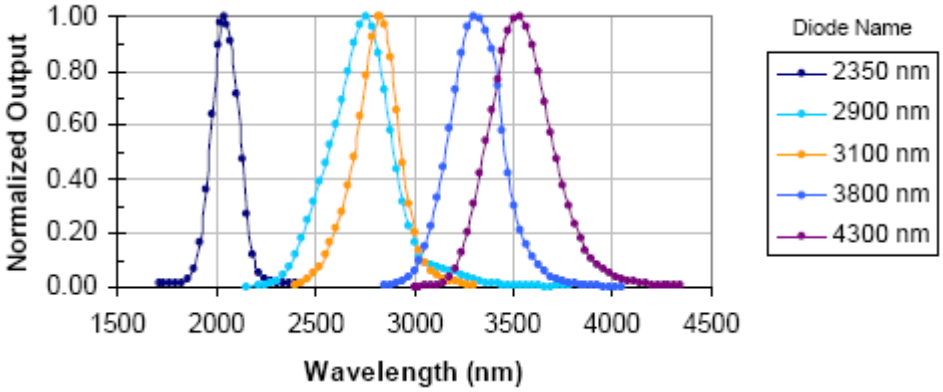

Figure 44: Relative output curves for the LEDs in the Arizona GL Dewar.

B2. Dewar Illumination Sources

The GL dewar is equipped with LEDs and a dome for illumination tests. These LEDs are thermally sunk to a surface held at the same temperature as the SCAs and so were operated at ~39K in these tests. Figure B1 shows relative output as a function of wavelength for the LEDS at 78K. The LEDs are referred to using their 300K wavelengths s as these are the names by which the LEDs are listed by the manufacturer. Only the 3100 nm and 4300nm LEDs from the set shown in Figure B1 are installed in the GL Dewar. The central wavelengths will be slightly shorter at 39K than at 78K. The LEDs can be switched on and off under computer control, and the currents used to drive them are also under computer control. Figure B2 shows a sample output versus input current for an LED -- shape of the curve is common for all LEDs but the amplitude varies by type.

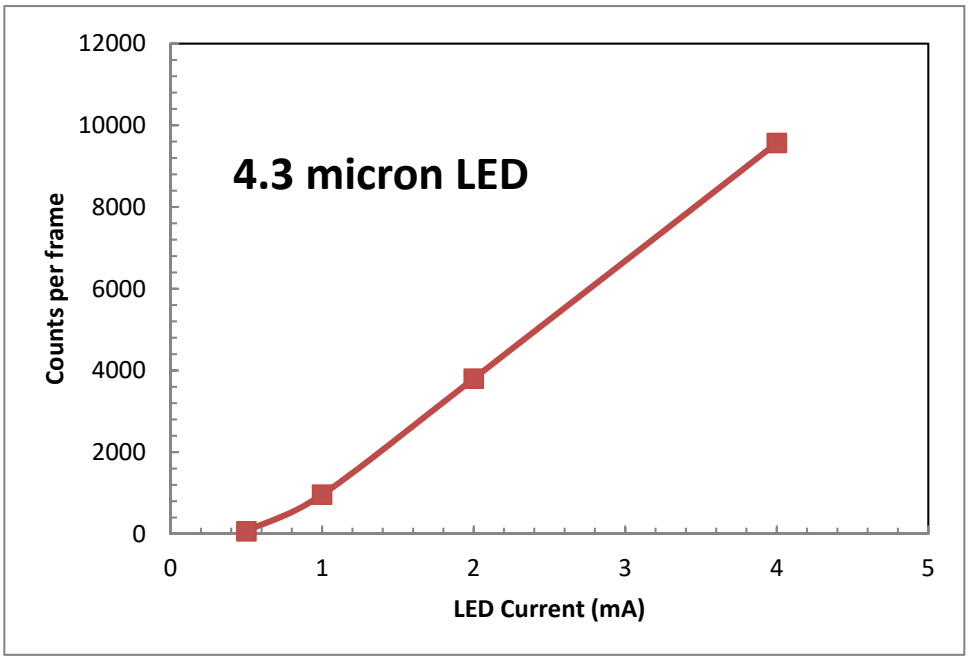

Figure 45: Detected output as a function of LED current.

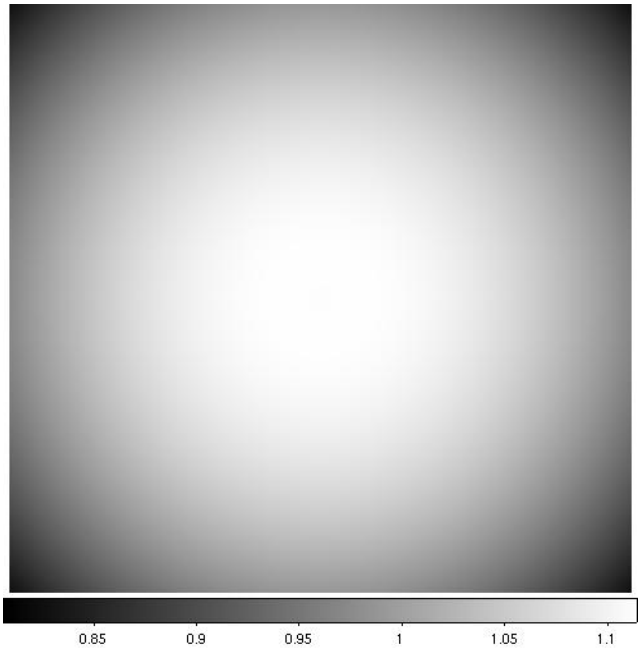

The dome in the GL dewar is located rather close to the LEDs themselves so a truly uniform illumination pattern is not possible. The actual illumination pattern produced by reflecting the LEDs off the dome was measured by taking one SCA and measuring its response at all four dewar locations. Figure 46 shows the derived illumination pattern over the entire field of view which was used to correct the measured SCA response to an approximate flat field. An LW FPA sees only the central one quarter of this pattern.

Figure 46: GL dewar illumination pattern.